

PED-ANOVA: Efficiently Quantifying Hyperparameter Importance in Arbitrary Subspaces

Shuhei Watanabe, Archit Bansal and Frank Hutter

Department of Computer Science, University of Freiburg, Germany

{watanabs,bansala,fh}@cs.uni-freiburg.de

Abstract

The recent rise in popularity of Hyperparameter Optimization (HPO) for deep learning has highlighted the role that good hyperparameter (HP) space design can play in training strong models. In turn, designing a good HP space is critically dependent on understanding the role of different HPs. This motivates research on HP Importance (HPI), e.g., with the popular method of functional ANOVA (f-ANOVA). However, the original f-ANOVA formulation is inapplicable to the subspaces most relevant to algorithm designers, such as those defined by top performance. To overcome this issue, we derive a novel formulation of f-ANOVA for arbitrary subspaces and propose an algorithm that uses Pearson divergence (PED) to enable a closed-form calculation of HPI. We demonstrate that this new algorithm, dubbed *PED-ANOVA*, is able to successfully identify important HPs in different subspaces while also being extremely computationally efficient.

1 Introduction

Following on the heels of widespread adoption of deep learning models in various industries and areas of research, Hyperparameter Optimization (HPO) [Bergstra and Bengio, 2012; Snoek *et al.*, 2012; Bergstra *et al.*, 2011; Lindauer *et al.*, 2022; Watanabe, 2023] for deep learning has gained increasing prominence as the path forward for making deep learning more accessible and robust. In particular, recent research has highlighted the role that good hyperparameter (HP) space design can play in training strong models [Chen *et al.*, 2018; Melis *et al.*, 2018; Henderson *et al.*, 2018]. In practice, while a large search space is necessary to find high-performance models [Zimmer *et al.*, 2021], a reduced search space that retains only important HPs is essential for efficiently finding them [Perrone *et al.*, 2019]. Therefore, it is crucial to understand the role that different HPs play in a search space.

This is the driving force behind previous research into the quantification of HP Importance (HPI) [Hutter *et al.*, 2014; Biedenkapp *et al.*, 2017], which still remains a largely understudied section of HPO research. Several HPO frameworks [Biedenkapp *et al.*, 2018; Akiba *et al.*, 2019; Sass

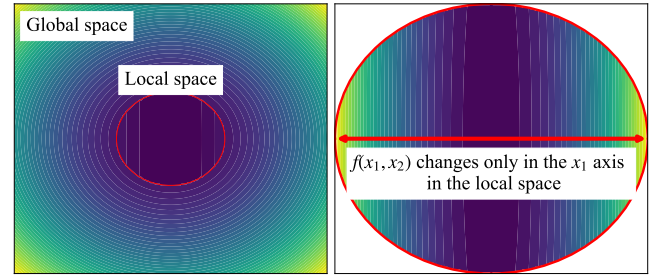
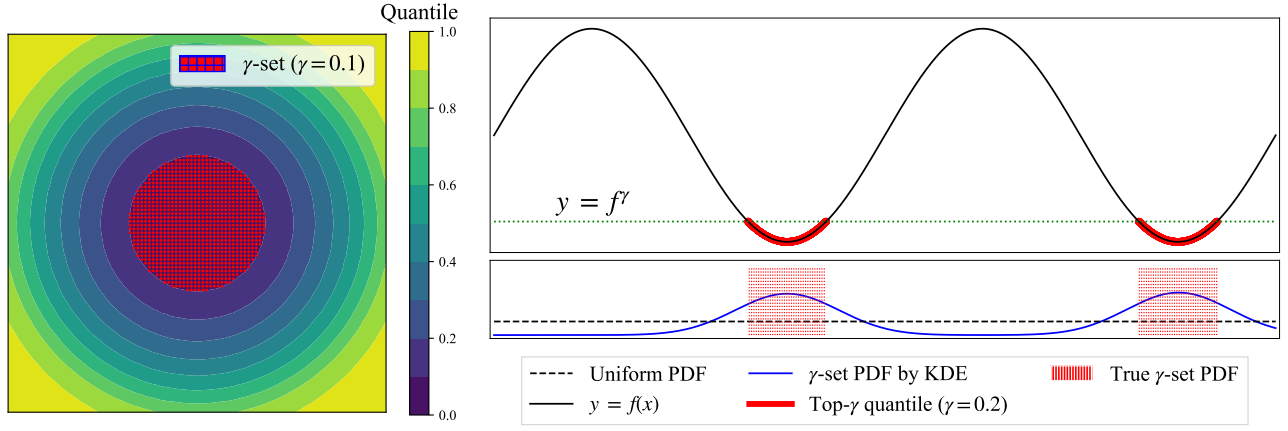


Figure 1: An example where the trend of HPI changes in the global and local space (top-10%). The horizontal axis is the x_1 -axis, the vertical axis is the x_2 -axis, and $f(x_1, x_2)$ is the objective function to analyze (darker is better). **Left:** the normalized contour plot of $f(x_1, x_2)$ in global space; both x_1 and x_2 appear to variate $f(x_1, x_2)$ equally. The red circle is the promising domain we would like to explore. **Right:** the normalized contour plot of $f(x_1, x_2)$ in the local space (the red circle in global space); $f(x_1, x_2)$ variates only by x_1 , and thus x_1 is more important. Such a trend cannot be captured by existing methods.

et al., 2022] have previously utilized functional ANOVA (f-ANOVA) [Hooker, 2007; Hutter *et al.*, 2014] to provide a better interpretation of the role of different HPs, but the original f-ANOVA formulation is not very practical for the interpretation of specific subspaces of a search space. Such subspaces are often of particular interest to algorithm developers due to various properties, for example, the “local space” visualized in Figure 1 could represent a region of high performance. Nevertheless, prior works [Hutter *et al.*, 2014; Biedenkapp *et al.*, 2018] have attempted to overcome this and quantify HPI in specific subspaces using f-ANOVA. However, since their formulation did not constrain the calculations to subspaces of high interest, we argue that the results are biased towards unimportant subspaces. At the same time, obtaining an unbiased quantification of HPI in specific subspaces of interest, which we refer to as *local* spaces in contrast to the full *global* space, is mathematically non-trivial.

To overcome this issue, we first formally define local HPI as HPI in a local space and we derive a novel formulation of f-ANOVA to compute local HPI for arbitrary local spaces. Still, our formulation would require Monte-Carlo sampling in general and it is computationally intractable. Therefore, we show that local HPI is tractable without a Monte-Carlo sampling under some constraints and propose an algorithm



(a) The true γ -set of $f(x_1, x_2) = x_1^2 + x_2^2$

(b) An empirical γ -set PDF using KDE of $f(x) = \sin x$

Figure 2: Conceptual visualizations of the γ -set and the γ -set PDF. **Left:** the true γ -set in a 2D example. Darker is better in the figure and we colored the top-10% in red, which is the γ -set \mathcal{X}^γ ($\gamma = 0.1$) in this example. **Right:** the true γ -set and the γ -set PDF in a 1D example. The green dotted line shows the γ -quantile value f^γ , which achieves the top-20% in this example, and the red solid lines are the γ -set \mathcal{X}^γ ($\gamma = 0.2$). The red dotted spaces below show the true γ -set PDF $p(\mathbf{x}|\mathcal{X}^\gamma)$, but since we do not have the analytical form in practice, this PDF is estimated by KDE (the blue solid line).

that uses Pearson divergence (PED, [Pearson, 1900]) to enable a closed-form computation of HPI. In a series of experiments, we first verify that our algorithm correctly provides global and local HPI in a toy function. Then we demonstrate that our algorithm takes only less than a second for 10^5 data points while the prior f-ANOVA [Hutter *et al.*, 2014] would take more than a week.

To provide a solid picture of how to use our method, we perform analysis on JAHS-Bench-201 [Bansal *et al.*, 2022], which has one of the largest search spaces among HPO benchmarks. In the analysis, we find that it is suboptimal to design a search space relying only on global HPI because we potentially miss important HPs in a local space if the global HPI of these HPs are dominated by the most important HP. We demonstrate that local HPI plays a crucial role to avoid this issue. Furthermore, our method has several other possible applications such as (1) post-hoc analysis for HPO, (2) adaptive (e.g., meta-learned) search space reductions for faster HPO, and (3) exploratory data analysis. We discuss these in more detail in Appendix E, along with the advantages and limitations of our method.

In summary, the contributions of this paper are to:

1. reformulate local HPI mathematically and derive the general formula of local HPI,
2. provide a closed-form calculation for local HPI using PED that handles even 10^8 data points in a minute, and
3. benchmark performance compared with the original f-ANOVA.

To facilitate reproducibility, our implementation is available at <https://github.com/nabenabe0928/local-anova/>.

2 Background & Related Work

2.1 Preliminaries

Throughout this paper, we use the following terms:

1. **γ -quantile value f^γ :** The function value $f^\gamma \in \mathbb{R}$ that achieves the top- γ quantile with respect to the objective function $f : \mathcal{X} \rightarrow \mathbb{R}$ to analyze in the global space \mathcal{X} ,
2. **γ -set \mathcal{X}^γ :** A set of configurations \mathcal{X}^γ that achieves the top- γ quantile in the global space \mathcal{X} , and
3. **Marginal γ -set PDF $p_d(x_d|\mathcal{X}^\gamma)$:** The marginal PDF of the γ -set PDF $p(\mathbf{x}|\mathcal{X}^\gamma)$:

$$p_d(x_d|\mathcal{X}^\gamma) := \int_{\mathbf{x}_{-d} \in \mathcal{X}_{-d}} p(\mathbf{x}|\mathcal{X}^\gamma) d\mathbf{x}_{-d}. \quad (1)$$

We provide the formal definitions in Appendix B and the conceptual visualizations in Figure 2. Note that $\mathcal{X} := \mathcal{X}_1 \times \dots \times \mathcal{X}_D$ is the search space, $\mathcal{X}_d \subseteq \mathbb{R}$ for $d \in [D] := \{1, \dots, D\}$ is the domain of the d -th HP, $\mathbf{x}_s \sim \mathcal{X}_s \subseteq \mathbb{R}^{|s|}$ denotes \mathbf{x}_s is sampled from the uniform distribution on \mathcal{X}_s where $s \subseteq [D]$, and $\mathcal{X}_{-d} \subseteq \mathbb{R}^{D-1}$ is \mathcal{X} without the d -th dimension. Furthermore, we consistently denote the PDF of the uniform distribution as *uniform PDF* and follow the assumptions stated in Appendix C.1.

2.2 f-ANOVA

In this section, we describe f-ANOVA for one-dimensional effects and refer to more details about the general version in Appendix A.3. Suppose we would like to quantify HPI of a function $f(\mathbf{x})$ defined on \mathcal{X} , then global HPI [Hooker, 2007] requires (see Figure 3 for the intuition):

1. **Global mean:**

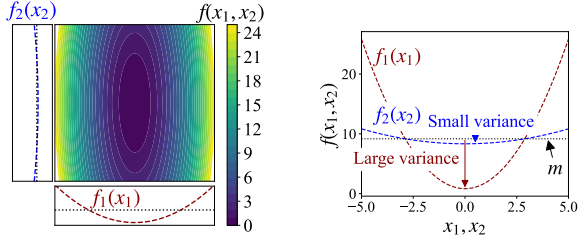
$$m := \mathbb{E}_{\mathbf{x} \sim \mathcal{X}}[f(\mathbf{x})], \quad (2)$$

2. **Marginal mean:**

$$f_d(x_d) := \mathbb{E}_{\mathbf{x}_{-d} \sim \mathcal{X}_{-d}}[f(\mathbf{x}|x_d)], \quad (3)$$

3. **Marginal variance:**

$$v_d := \mathbb{E}_{x_d \sim \mathcal{X}_d}[(f_d(x_d) - m)^2]. \quad (4)$$



(a) The contour plot of $f(x_1, x_2) = x_1^2 + x_2^2/10$ and the marginal means for each dimension. (b) The conceptual visualization of global HPI on $f(x_1, x_2) = x_1^2 + x_2^2/10$.

Figure 3: The conceptual visualization of global HPI on $f(x_1, x_2) = x_1^2 + x_2^2/10$. **Left:** the landscape of $f(x_1, x_2)$ (darker is better) and the marginal means $f_1(x_1)$ and $f_2(x_2)$. The color does not change a lot in the vertical direction (the x_2 -axis) while it does in the horizontal direction (the x_1 -axis). **Right:** the marginal means and the mean value in the same plane. As the marginal mean f_1 (the red dashed line) has a large variance, x_1 is more important. On the other hand, as the marginal mean f_2 (the blue dashed line) has a small variance, x_2 is less important.

Note that $f(\mathbf{x}|x_d)$ implies that we fix the d -th HP of \mathbf{x} to x_d . When we denote the global variance as v_0 , the ratio v_d/v_0 is the *global HPI* of the d -th HP and in essence, the magnitude of the marginal variance represents the relative importance.

2.3 Local f-ANOVA in Prior Works

To the best of our knowledge, there are two papers that mention *local HPI* (and both use f-ANOVA). Hutter *et al.* [2014] mentioned local HPI can be quantified by taking:

$$g(\mathbf{x}) := \min(f(\mathbf{x}), f^\gamma); \quad (5)$$

however, since this measure is biased depending on the global space design as discussed in Appendix B.4.1, we need to consider the integral only over a local space as stated in Section 3.1. Biedenkapp *et al.* [2018] proposed the following HPI measure:

$$\begin{aligned} m_d &:= \mathbb{E}_{x_d \sim \mathcal{X}_d} [f(\mathbf{x}|x_d^{\text{opt}})], \\ v_d &:= \mathbb{E}_{x_d \sim \mathcal{X}_d} [(f(\mathbf{x}|x_d^{\text{opt}}) - m_d)^2], \end{aligned} \quad (6)$$

where $\mathbf{x}^{\text{opt}} \in \mathbb{R}^D$ is the optimized setting and $\mathbf{x}_{-d}^{\text{opt}} \in \mathbb{R}^{D-1}$ is \mathbf{x}^{opt} without the d -th dimension. The authors mention that this measure is a local HPI measure; however, this measure is also not a local HPI measure in our definition and we show that this is the case using a toy example in Appendix B.4.2.

3 Local f-ANOVA Using Pearson Divergence

In this section, we first provide the definition of local HPI and describe how to define a local space. For simplicity, we name this local space definition as *Lebesgue split*¹. Then we introduce fast algorithm using PED between two KDEs to compute local HPI and benchmark the speed of the algorithm

¹The name comes from the fact that we define a local space by a function value as in the Lebesgue integral in contrast to the definition of a local space by bounds for each dimension, which we name *Riemann split*.

compared to the f-ANOVA implementation based on random forests [Hutter *et al.*, 2014]. Notice that since higher orders of HPI require exponential amounts of computations and usually lack interpretability, our discussion does not focus on higher orders; however, we derive the formula for higher orders and show them in Eqs. (47), (52) in Appendix C. The theoretical details for this section are available in Appendix B.

3.1 Local Hyperparameter Importance

In this section, we assume that we have a set of (sorted) observations $\mathcal{D} := \{(\mathbf{x}_n, f(\mathbf{x}_n))\}_{n=1}^N$ such that $f(\mathbf{x}_1) \leq \dots \leq f(\mathbf{x}_N)$. Then, the top- γ -quantile observations are $\mathcal{D}^\gamma = \{(\mathbf{x}_n, f(\mathbf{x}_n))\}_{n=1}^{\lceil \gamma N \rceil}$ and the γ -quantile value is $f^\gamma := f(\mathbf{x}_{\lceil \gamma N \rceil})$.

3.1.1 Local Space Defined by Lebesgue Split

To begin with, we formally define local HPI:

Definition 1 (Local HPI) Given a subspace $\mathcal{X}^* \subseteq \mathcal{X}$, local HPI is global HPI v_d/v_0 in the subspace \mathcal{X}^* .

Recall that v_d is the marginal variance of the d -th HP and v_0 is the global variance. Based on Definition 1, the prior works on making f-ANOVA local discussed in Section 2.3 are not local HPI measures; see Appendix B.4 for more details. As our local HPI obviously depends on the choice of \mathcal{X}^* , local HPI is a very general concept; therefore, we focus on the so-called *Lebesgue split* to specify a local space in this paper. In the Lebesgue split, we obtain a local space \mathcal{X}^* as follows:

1. Fix a threshold f^* (we use the γ -quantile value f^γ in this paper instead), and
2. Obtain the sublevel set $\mathcal{X}^* := \{\mathbf{x} \in \mathcal{X} | f(\mathbf{x}) \leq f^*\}$ based on f^* (\mathcal{X}^* becomes the γ -set \mathcal{X}^γ when $f^* = f^\gamma$).

Recall that the definitions of the γ -quantile value and the γ -set are available in Section 2.1. More intuitively, the red domains in Figure 2 are the local space of each example. In this paper, we use $f(\mathbf{x}_{\lceil \gamma N \rceil})$ as f^γ . The advantages of the Lebesgue split are to:

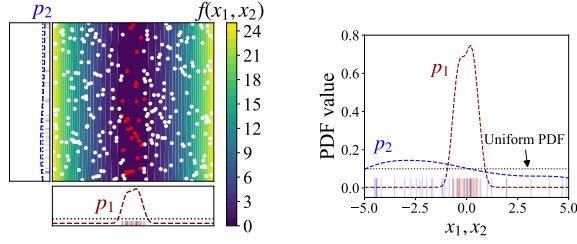
1. require only one parameter f^* while the Riemann split, which we split along each dimension by specifying bounds, requires at least $2 \times D$ parameters,
2. be able to focus on the analysis in promising domains where we are interested, and
3. be able to remove the sampling bias caused by a non-uniform sampler when using the formula of local HPI.

We further discuss the strengths and drawbacks of the Lebesgue split compared to the Riemann split in Appendix B.5.

3.1.2 Formula of Local Hyperparameter Importance

Now we discuss the computation of local HPI. In Eqs. (2)–(4), we take the expectation over the uniform distribution of the global space \mathcal{X} . In the same vein, it is natural to consider the expectation over the uniform distribution of the local space \mathcal{X}^γ for local HPI as well. Although the computation is not obvious, we can compute the expectation of a measurable function $f(\mathbf{x})$ over the local space \mathcal{X}^γ if we use the following trick:

$$\frac{1}{\gamma} \mathbb{E}_{\mathbf{x} \sim \mathcal{X}} [f(\mathbf{x}) \mathbb{I}[\mathbf{x} \in \mathcal{X}^\gamma]], \quad (7)$$



(a) The contour plot of $f(x_1, x_2)$ and the marginal γ' -set PDFs. (b) The conceptual visualization of global HPI by PED.

Figure 4: The conceptual visualization of global HPI using PED on $f(x_1, x_2) = x_1^2 + x_2^2/100$. As we consider global HPI in this example, the γ -set PDF is the uniform PDF. **Left:** the landscape of $f(x_1, x_2)$ (darker is better) and the marginal γ' -set PDFs $p_1(x_1|\mathcal{D}^{\gamma'})$ ($= p_1$, the red dashed line) and $p_2(x_2|\mathcal{D}^{\gamma'})$ ($= p_2$, the blue dashed line). The dots represent observations (datasets) and the red dots achieve the top- γ' quantile. p_1, p_2 are estimated by Eq. (15) using the red dots. **Right:** the marginal γ' -set PDFs in the same plane. While p_1 (the red dashed line) sharply peaks at the center, p_2 (blue dashed line) is close to the uniform PDF. This implies that the latter is closer to the uniform PDF, and thus x_2 is less important.

where $\gamma = \mathbb{E}_{\mathbf{x} \sim \mathcal{X}}[\mathbb{I}[\mathbf{x} \in \mathcal{X}^\gamma]]$ is a normalization constant. Recall that $\mathbf{x} \in \mathcal{X}^\gamma$ and $f(\mathbf{x}) \leq f^\gamma$ are equivalent. Similarly, the marginal mean of $f(\mathbf{x})$ is computed as follows:

$$\frac{1}{V_d^\gamma(x_d)} \mathbb{E}_{\mathbf{x}_{-d} \sim \mathcal{X}_{-d}}[f(\mathbf{x}|\mathbf{x}_{-d})\mathbb{I}[\mathbf{x} \in \mathcal{X}^\gamma|\mathbf{x}_{-d}]], \quad (8)$$

where $V_d^\gamma(x_d) := \mathbb{E}_{\mathbf{x}_{-d} \sim \mathcal{X}_{-d}}[\mathbb{I}[\mathbf{x} \in \mathcal{X}^\gamma|\mathbf{x}_{-d}]]$ is a normalization constant. Then local HPI is generally computed as follows:

1. Local mean:

$$m^\gamma := \frac{1}{\gamma} \mathbb{E}_{\mathbf{x} \sim \mathcal{X}}[f(\mathbf{x})\mathbb{I}[\mathbf{x} \in \mathcal{X}^\gamma]], \quad (9)$$

2. Local marginal mean:

$$f_d^\gamma(x_d) := \frac{1}{V_d^\gamma(x_d)} \mathbb{E}_{\mathbf{x}_{-d} \sim \mathcal{X}_{-d}}[f(\mathbf{x}|\mathbf{x}_{-d})\mathbb{I}[\mathbf{x} \in \mathcal{X}^\gamma|\mathbf{x}_{-d}]], \quad (10)$$

3. Local marginal variance:

$$v_d^\gamma := \mathbb{E}_{x_d \sim V_d^\gamma}[(f_d^\gamma(x_d) - m^\gamma)^2]. \quad (11)$$

Note that $x_d \sim V_d^\gamma$ implies that x_d is sampled from the distribution of the PDF $V_d^\gamma(x_d)/Z$ where $Z \in \mathbb{R}_+$ is the normalization constant. As the series of computations requires a Monte-Carlo sampling in a $D - 1$ dimensional space, the time complexity incurs the curse of dimensionality. In the next section, we introduce fast algorithm to compute local HPI in exchange for the scale ignorance.

3.2 Fast Algorithm by Pearson Divergence

If we analyze the binary function $b(\mathbf{x}|\mathcal{X}^{\gamma'}) := \mathbb{I}[\mathbf{x} \in \mathcal{X}^{\gamma'}] = \mathbb{I}[f(\mathbf{x}) \leq f^{\gamma'}]$ instead of $f(\mathbf{x})$, HPI can be efficiently computed where $\gamma'(< \gamma)$ is another quantile to define the binary function in the local space \mathcal{X}^γ . First, we prove the following theorem:

Algorithm 1 Local PED-ANOVA

$\mathcal{D} = \{(\mathbf{x}_n, f(\mathbf{x}_n))\}_{n=1}^N$ (Dataset to analyze), γ, γ' (User-defined quantiles of top domains)

- 1: \triangleright See Appendices E.2, E.3 for practical usages
- 2: Sort \mathcal{D} in ascending order by f
- 3: $\triangleright |\mathcal{D}^\gamma| \geq 2$ and $|\mathcal{D}^{\gamma'}| \geq 2$ must hold
- 4: Pick the top- γ and $-\gamma'$ quantile observations $\mathcal{D}^\gamma, \mathcal{D}^{\gamma'}$
- 5: **for** $d = 1, \dots, D$ **do**
- 6: Count occurrences of unique values $c_d^{(n)}$
- 7: Build KDEs $p_d(\cdot|\mathcal{D}^\gamma), p_d(\cdot|\mathcal{D}^{\gamma'})$ by Eq. (15)
- 8: Compute v_d^γ by Eq. (16)
- 9: **return** $\{v_d^\gamma\}_{d=1}^D$

Theorem 1 Given the binary function $b(\mathbf{x}|\mathcal{X}^{\gamma'})$ and the γ' - and γ -set PDFs $p(\mathbf{x}|\mathcal{X}^{\gamma'}), p(\mathbf{x}|\mathcal{X}^\gamma)$ where $\gamma' < \gamma$, the local marginal variance of each dimension $d \in [D]$ is:

$$v_d^\gamma = \left(\frac{\gamma'}{\gamma}\right)^2 D_{\text{PE}}(p_d(\cdot|\mathcal{X}^{\gamma'})||p_d(\cdot|\mathcal{X}^\gamma)). \quad (12)$$

The proof is provided in Appendix C.3 and higher orders of HPI can be computed by Eq. (52) in Appendix C.3. Note that PED between the PDFs p, q defined on \mathcal{X}_d is computed as:

$$D_{\text{PE}}(p||q) := \mathbb{E}_{x_d \sim q(x_d)} \left[\left(\frac{p(x_d)}{q(x_d)} - 1 \right)^2 \right]. \quad (13)$$

As we do not have the ground truth of the marginal γ' - and γ -set PDFs, we replace them with KDEs. The tricks of this computation are that (1) the marginal γ -set PDF can be easily estimated by (1D) KDE as follows and (2) we only need to take the average in 1D space:

$$p_d(x_d|\mathcal{D}^\gamma) := \frac{1}{|\gamma N|} \sum_{n=1}^{|\gamma N|} k(x_{n,d}, x_d). \quad (14)$$

Note that $x_{n,d} \in \mathcal{X}_d$ is the d -th dimension of \mathbf{x}_n and k is a kernel function. Although the query of this function still requires $O(N)$, the time complexity scales down to $O(n_d)$ where $n_d \in \mathbb{Z}_+$ is the number of unique values in the d -th HP if we use the following compression:

$$p_d(x_d|\mathcal{D}^\gamma) = \frac{1}{|\gamma N|} \sum_{n=1}^{n_d} c_d^{(n)} k(x_d^{(n)}, x_d) \quad (15)$$

where $x_d^{(n)}$ is the n -th unique value in the d -th HP and $c_d^{(n)}$ is the occurrences of this value in \mathcal{D}^γ . Note that we discretize a continuous HP $x_d \in [L, R]$ ($L < R$) (if exists) as $x_d \in \{L + n(R - L)/(n_d - 1)\}_{n=0}^{n_d-1}$ to apply Eq. (15) and the discretization error of marginal variances is bounded by $O(\frac{1}{n_d})$ under some assumptions. Since we can avoid Monte-Carlo samplings with the discretization and the total time complexity is reduced to $O(N + n_d^2)$, this is a trade-off; see Proposition 2 in Appendix C.4 for more details. Hence Eq. (11) is approximated as the following closed-form:

$$v_d^\gamma \simeq \left(\frac{\gamma'}{\gamma}\right)^2 \sum_{n=1}^{n_d} \frac{p_d(x_d^{(n)}|\mathcal{D}^\gamma)}{Z} \left(\frac{p_d(x_d^{(n)}|\mathcal{D}^{\gamma'})}{p_d(x_d^{(n)}|\mathcal{D}^\gamma)} - 1 \right)^2 \quad (16)$$

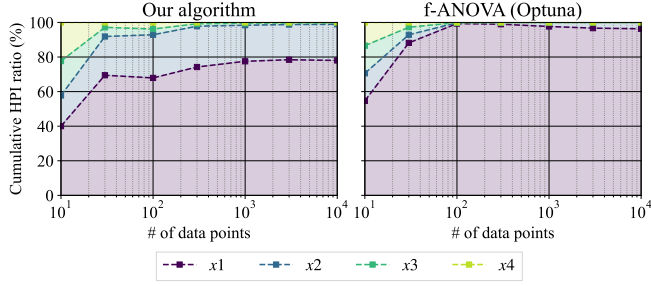


Figure 5: The comparison of global HPI between our algorithm (**Left**) and Optuna f-ANOVA (**Right**). HPI is averaged over 10 runs with different random seeds. The horizontal axis shows the number of data points N and the vertical axis shows the cumulative HPI ratio. HPI ratio is computed by $v_d / \sum_{d'=1}^D v_{d'}$ and the weak color band between each plot shows the HPI ratio of each HP.

where $Z := \sum_{n=1}^{n_d} p_d(x_d^{(n)} | \mathcal{D}^\gamma)$ is a normalization constant and the time complexity of this computation is $O(n_d^2)$. Algorithm 1 shows the pseudocode for the local HPI computation. Note that global HPI, whose computation is detailed in Appendix B.2, can be computed by replacing $p_d(\cdot | \mathcal{D}^\gamma)$ with the uniform PDF in the d -th dimension $u_d(x_d)$ (or $p_d(\cdot | \mathcal{D}^\gamma)$ with $\gamma = 1$, i.e. $p_d(\cdot | \mathcal{D})$, as discussed in Appendix E.2 when collecting \mathcal{D} by a non-uniform sampler). Figure 4 presents an example of global HPI with our method on a 2D toy function.

4 Performance Validation

4.1 Setup

In this section, we consistently use the following function:

$$f(x_1, x_2, x_3, x_4) = \sum_{d=1}^4 w_d(x_d) \times x_d^2 \quad (17)$$

where $x_d \in [-5, 5]$ for all $d \in \{1, 2, 3, 4\}$ and the weights $w_d : \mathbb{R} \rightarrow \mathbf{W}$ follow:

$$w_d(x) = \begin{cases} W_{d-1} & (|x| \geq 1) \\ W_{d+2 \bmod 4} & (\text{otherwise}) \end{cases} \quad (18)$$

and $\mathbf{W} := \{W_d\}_{d=0}^3 = \{5^0, 5^{-1}, 5^{-2}, 5^{-3}\}$. This function has different trends of HPI in global and local spaces. While the order of HPI is x_1, x_2, x_3, x_4 in the global space, it is x_2, x_3, x_4, x_1 in the local space $\{x \in \mathcal{X} | \forall d \in [4], |x_d| < 1\}$.

In this experiment, we discretized the HPs with $n_d = 1001$ and all samples were drawn from the uniform distribution. Furthermore, all experiments were run on the hardware with Intel Core i7-10700 and we used the f-ANOVA implementation with the default parameter setting by Optuna². Note that the Optuna implementation is based on Hutter *et al.* [2014].

4.2 Effect of Scale Ignorance in Global HPI

Since PED-ANOVA uses $\mathbb{I}[f(x) \leq f^*]$ instead of $f(x)$, it cannot capture scale information. On the other hand, since our objective is to identify important HPs, we would like to test if PED-ANOVA can identify important HPs. In the experiment, we used $\gamma' = 0.1$. Figure 5 shows the cumulative

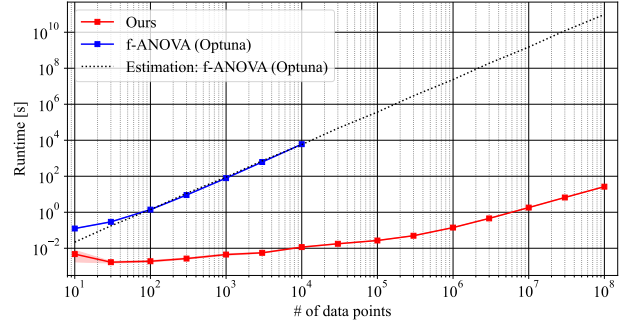


Figure 6: The benchmark of query speed of our method and f-ANOVA with respect to the number of data points N . Each setting was run with 10 different seeds and the weak color bands show the standard error. As f-ANOVA requires much more computation, we estimated the evolution and provided the estimation by the black dotted line.

global HPI ratio of each method. As seen in the figure, while both methods could identify the most important HP x_1 , we can see the difference in the HPI of x_2 . While PED-ANOVA tells us x_2 has about 20% of contribution to achieve the top-10%, f-ANOVA tells us x_2 has about 3% of contribution. This difference comes from whether we ignore the scale of the objective function or not. Since f-ANOVA considers scale and it magnifies the contribution in the tail of the function, it dilutes the HPI of x_2 , which has less weight in the tail. Note that “tail” refers to the domains that cause a lot of variations, yet not critical for the final result, in the objective function f and $|x_d| \geq 1$ is the tail in our case; more details in Appendix B.6. On the other hand, the HPI of x_1 by PED-ANOVA is not strongly biased by the tail due to the scale ignorance nature. This leads to more importance in x_2 . Although our method loses scale information, the ignorance of scale allows us to abandon the information from the tail and focus only on the information from the promising domain, which is γ' -set in our case. Furthermore, this remarkable property makes the meaning of HPI, which is how important each HP is to achieve the top- γ' quantile, very clear and practitioners can extract the nuance of each HP for specific local spaces.

4.3 Query Speed

As mentioned previously, one of the benefits of our method is the query speed, and we would like to benchmark how quick our method is in this section. In the experiment, we used $\gamma' = 0.1$. Figure 6 presents the runtime with respect to the number of data points. While f-ANOVA requires more than a minute with 10^3 data points and more than a week with 10^5 data points, our method provides the results in a minute even with 10^8 data points. In Appendix D.2, we test our method with higher dimensionality to see the number of data points required for convergence.

4.4 Local Importance Measure

Finally, we check if our method can successfully identify important HPs in promising domains. The objective function $f(x)$ is designed so that while x_1 is important and x_3 is trivial in the global space, x_1 is less important and x_3 is important in the local space. The goal of this experiment is to check

²<https://github.com/optuna/optuna>

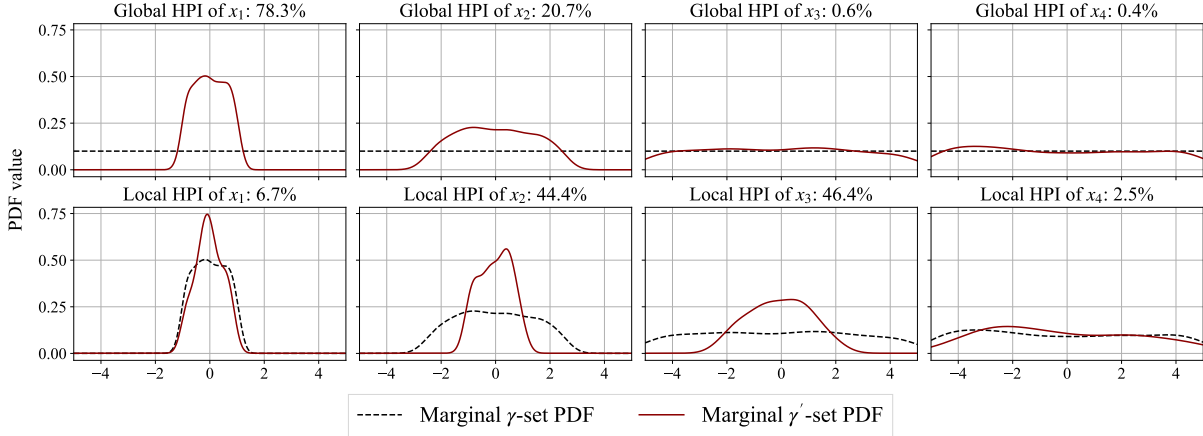


Figure 7: The validation of the local importance measure. The black dashed lines show the marginal γ -set PDFs and the red lines show the marginal γ' -set PDFs for each dimension. The percentage (**HPI ratio**) was computed by $v_d / \sum_{d'=1}^D v_{d'}$. **Top row**: the plots of the uniform PDFs ($\gamma = 1$) and the marginal $\gamma' = 0.1$ -set PDFs. These are used to compute global HPI. **Bottom row**: the plots of the marginal $\gamma = 0.1$ -set PDFs and the marginal $\gamma' = 0.01$ -set PDFs. Those are used to compute local HPI in the top-10% domain.

Table 1: HPI of CIFAR10 in JAHS-Bench-201. The ratio of HPI by percentage (**HPI ratio**) computed by $v_d / \sum_{d'=1}^D v_{d'}$. The top-3 HPs are bolded. **Cols. 1,3,5** (Original): HPI by f-ANOVA on $g(\mathbf{x}) := \min(f(\mathbf{x}), f^{\gamma'})$. **Cols. 2,4,6** (Ours): HPI by PED-ANOVA.

Hyperparameter	Normal Original	HPI ratio (%)					
		Global 0.1		Global 0.01		Local	
		Ours	Original	Ours	Original	Ours	
Learning rate	1.36	9.11	10.20	6.62	3.59	4.09	
Weight decay	0.96	2.19	0.68	2.56	0.31	3.00	
Activation function	0.01	0.12	0.21	0.26	0.41	0.40	
TrivialAugment	0.00	4.33	3.83	13.22	8.27	28.33	
Depth multiplier	0.06	0.66	0.58	2.47	0.63	6.90	
Width multiplier	1.60	60.22	73.59	35.26	71.75	9.07	
Operation 1 (Op.1)	11.86	6.65	3.45	11.95	3.81	13.38	
Operation 2 (Op.2)	4.04	2.36	1.42	5.00	2.51	6.97	
Operation 3 (Op.3)	64.73	5.63	1.14	5.25	1.73	5.50	
Operation 4 (Op.4)	0.09	0.84	0.83	1.62	1.09	2.09	
Operation 5 (Op.5)	4.00	2.19	1.04	4.72	1.29	6.76	
Operation 6 (Op.6)	11.29	5.71	3.02	11.06	4.61	13.52	

whether our method can provide this insight. In the experiment, we used $N = 10^4$.

Figure 7 shows the results. As discussed already, global HPI could identify the order of HPI appropriately. For local HPI, our method could tell us that x_2, x_3 are the most important HPs in the local space and x_1 is less important as expected. Note that since the $\gamma = 0.1$ -set already narrows down the domain of x_2 , but not x_3 , this dilutes the HPI of x_2 and increases the HPI of x_3 . Prior works cannot provide this interpretation as discussed in Appendix B.4.

5 Real-World Usecase by JAHS-Bench-201

5.1 Setup

In order to further verify our proposed algorithm against a real-world application, we applied PED-ANOVA to analyze the search space of JAHS-Bench-201 [Bansal *et al.*, 2022], which is a surrogate benchmark for HPO and has a very large search space in the context of extant HPO benchmarks. We constructed the dataset \mathcal{D} in Algorithm 1 by querying JAHS-Bench-201 for the validation accuracy, i.e. $f(\mathbf{x})$, of N lattice points, where $N = 41,343,750$, generated by discretiz-

ing the JAHS-Bench-201 search space (see Table 2 of Appendix D.1). Although JAHS-Bench-201 can be queried for model performance metrics on 3 different image classification datasets, for the sake of brevity, we discuss only the experiments performed on CIFAR10 here and include the results on the other datasets in Appendix D.3. Due to the computational complexity of f-ANOVA, we could use only 10^4 data points for it, in contrast to PED-ANOVA, and calculated the mean of HPI over 10 independent runs. Since the surrogate models in JAHS-Bench-201 are trained XGBoost models and XGBoost’s outputs are deterministic, we query each lattice point only once. In the analysis, we would like to answer the following research questions (RQs):

- RQ1:** Does global HPI of our method provide the same important HPs as f-ANOVA with Eq. (5)?
- RQ2:** Is the scale ignorance necessary for matching the intuition of achieving the top- γ' quantile?
- RQ3:** Does local HPI help detect potentially important HPs or trivial HPs?

In order to answer RQs, we provide Table 1 with the HPI of each HP in CIFAR10 of JAHS-Bench-201 and Figure 8 to visualize the $\gamma = 0.1$ - and $\gamma = 0.01$ -set PDFs as the blue and the red shadows, respectively. Strictly speaking, discrete probability distributions are not PDFs due to discrete space; however, we use the term γ -set PDF for the sake of consistency. We applied f-ANOVA to $f(\mathbf{x})$ (Normal), $\min(f(\mathbf{x}), f^{\gamma'=0.1})$ (Global 0.1), and $\min(f(\mathbf{x}), f^{\gamma'=0.01})$ (Global 0.01), and PED-ANOVA with $\gamma' = 0.1$ (Global 0.1), $\gamma' = 0.01$ (Global 0.01), and $\gamma = 0.1, \gamma' = 0.01$ (Local). Recall that Global 0.1 and Global 0.01 for f-ANOVA are based on Eq. (5) and $f^{\gamma'=0.1}$ means $f_{[\lceil \mathcal{D} \rceil / 10]}$ given a dataset sorted by f_n . Although we used the uniform PDF to compute global HPI in this experiment, practitioners should use $p_d(\cdot | \mathcal{D})(\gamma = 1)$ instead of the uniform PDF for the post-hoc analysis of HPO when using a non-uniform sampler (e.g. Bayesian optimization) to remove sampling bias as discussed in Appendix E.2.

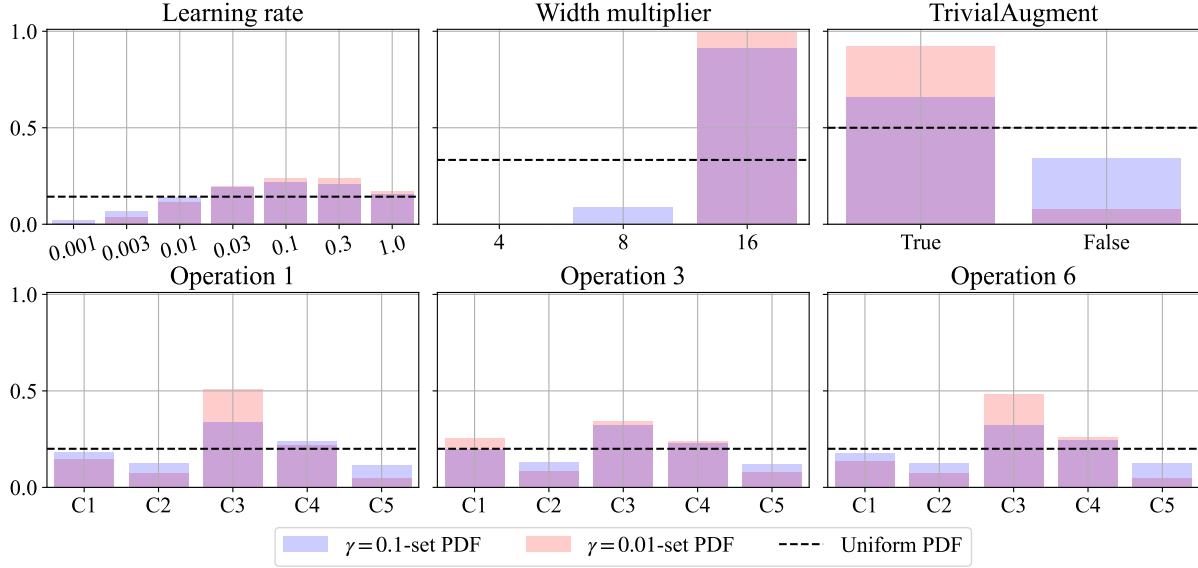


Figure 8: The distributions of important HPs of CIFAR10 in JAHS-Bench-201. The red shadows show the $\gamma = 0.01$ -set PDFs, the blue shadows show the $\gamma = 0.1$ -set PDFs, and the black dashed lines show the uniform PDFs. PED between a black line and a blue shadow is Global 0.1, PED between a black line and a red shadow is Global 0.01, and PED between a red shadow and a blue shadow is Local in Table 1. The titles for each figure show the names of each HP and the details of HPs are available in Appendix D.1. Notice that C1 – C5 correspond to the order of Table 2 and the overlap between the red and the blue shadows looks purple although they are separated shadows.

5.2 Analysis & Interpretation

To answer RQ1, we compare the column (Global 0.1, Ours) to (Global 0.1, Original) and the column (Global 0.01, Ours) to (Global 0.01, Original) in Table 1. We observe that both PED-ANOVA and f-ANOVA indicated the same top-2 important HPs although the 3rd-best HPs slightly varied. This result further verifies the validation in Section 4.2.

To answer RQ2, we discuss the results of (Global 0.1, Ours) and (Global 0.01, Ours) in the context of (Normal, Original) to assess the impact that the tail of $f(x)$ discussed in Section 4.2 has on f-ANOVA. The most important takeaway from this comparison is the misclassification of Op.3 as the most important and of TrivialAugment as the least important HP to optimize over by the original f-ANOVA in the global setting. As can be verified by looking at the γ -set PDFs, even for $\gamma = 0.01$, Op.3’s values are distributed very evenly even when TrivialAugment and Width multiplier have already shown convergence. This clearly indicates that Op.3 is not very important to optimize for achieving the top-1% performance and may or may not become relevant in even higher quantile regimes. At the same time, both columns’ values agree on the importance of Op.1 and Op.6. Therefore, to answer RQ2, scale invariance indeed helps to successfully identify HPI for HPs that would have been misclassified by the (Normal, Original) setting.

Finally, for RQ3, we compare the column (Global 0.01, Ours) to (Local, Ours). We observe that the HPI of Width multiplier drops sharply from the Global 0.01 setting to the Local setting. Simultaneously, the HPI of TrivialAugment increases sharply across the same. This suggests that optimizing Width

multiplier is no longer important when moving from the top-10% to the top-1% performance but optimizing TrivialAugment is very important. The reason behind this change becomes clear when we observe the change in γ -set PDFs of the two HPs in Figure 8. Both the γ -set PDFs for Width multiplier are sharply peaked at 16, indicating that no further optimization is needed on Width multiplier. However, the γ -set PDFs for TrivialAugment only start peaking at the value True for the $\gamma = 0.01$ -set PDF. This clearly demonstrates that local HPI is necessary for deriving the correct interpretation in the top- γ' quantiles, since (Local, Ours) successfully identifies the relative importance of optimizing the two HPs. Last but not least, if both global and local HPI with wished quantiles γ, γ' exhibits low values, removing such HPs, e.g. Activation function, is expected to have a less negative impact although it is insecure to remove HPs, e.g. Op.1, only by looking at global HPI.

6 Conclusions

In this paper, we reformulated f-ANOVA for local HPI and introduced the fast algorithm to compute local HPI by PED. In the series of experiments on a toy function, we confirmed that our method can quantify both global and local HPI appropriately, and efficiently compute HPI in a second with 10^5 data points while the prior work takes several days. In the analysis of JAHS-Bench-201, we provided a concrete example of how to use our method on benchmark datasets and showed that only using global HPI could be misleading. Due to the space limit, we defer a discussion of practical usecases and limitations of our method to Appendix E. Our implementation is available at <https://github.com/nabenabe0928/local-anova/>.

Acknowledgments

The authors appreciate the valuable contributions of the anonymous reviewers. Robert Bosch GmbH is acknowledged for financial support. The authors also acknowledge funding by European Research Council (ERC) Consolidator Grant “Deep Learning 2.0” (grant no. 101045765). Views and opinions expressed are however those of the authors only and do not necessarily reflect those of the European Union or the ERC. Neither the European Union nor the ERC can be held responsible for them.



Funded by
the European Union

References

- [Akiba *et al.*, 2019] T. Akiba, S. Sano, T. Yanase, T. Ohta, and M. Koyama. Optuna: A next-generation hyperparameter optimization framework. In *International Conference on Knowledge Discovery & Data Mining*, 2019.
- [Bansal *et al.*, 2022] A. Bansal, D. Stoll, M. Janowski, A. Zela, and F. Hutter. JAHS-Bench-201: A foundation for research on joint architecture and hyperparameter search. In *Advances in Neural Information Processing Systems Datasets and Benchmarks Track*, 2022.
- [Bergstra and Bengio, 2012] J. Bergstra and Y. Bengio. Random search for hyper-parameter optimization. *Journal of Machine Learning Research*, 13, 2012.
- [Bergstra *et al.*, 2011] J. Bergstra, R. Bardenet, Y. Bengio, and B. Kégl. Algorithms for hyper-parameter optimization. In *Advances in Neural Information Processing Systems*, 2011.
- [Biedenkapp *et al.*, 2017] A. Biedenkapp, M. Lindauer, K. Eggenberger, F. Hutter, C. Fawcett, and H. Hoos. Efficient parameter importance analysis via ablation with surrogates. In *Association for the Advancement of Artificial Intelligence*, 2017.
- [Biedenkapp *et al.*, 2018] A. Biedenkapp, J. Marben, M. Lindauer, and F. Hutter. CAVE: Configuration assessment, visualization and evaluation. In *International Conference on Learning and Intelligent Optimization*, 2018.
- [Chen *et al.*, 2018] Y. Chen, A. Huang, Z. Wang, I. Antonoglou, J. Schrittwieser, D. Silver, and N. de Freitas. Bayesian optimization in AlphaGo. *arXiv:1812.06855*, 2018.
- [Henderson *et al.*, 2018] P. Henderson, R. Islam, P. Bachman, J. Pineau, D. Precup, and D. Meger. Deep reinforcement learning that matters. In *Association for the Advancement of Artificial Intelligence*, 2018.
- [Hooker, 2007] G. Hooker. Generalized functional ANOVA diagnostics for high-dimensional functions of dependent variables. *Journal of Computational and Graphical Statistics*, 16, 2007.
- [Hutter *et al.*, 2014] F. Hutter, H. Hoos, and K. Leyton-Brown. An efficient approach for assessing hyperparameter importance. In *International Conference on Machine Learning*, 2014.
- [Lindauer *et al.*, 2022] M. Lindauer, K. Eggenberger, M. Feurer, A. Biedenkapp, D. Deng, C. Benjamins, T. Ruhkopf, R. Sass, and F. Hutter. SMAC3: A versatile bayesian optimization package for Hyperparameter Optimization. *Journal of Machine Learning Research*, 23, 2022.
- [Melis *et al.*, 2018] G. Melis, C. Dyer, and P. Blunsom. On the state of the art of evaluation in neural language models. In *International Conference on Learning Representations*, 2018.
- [Pearson, 1900] K. Pearson. On the criterion that a given system of deviations from the probable in the case of a correlated system of variables is such that it can be reasonably supposed to have arisen from random sampling. *Philosophical Magazine and Journal of Science*, 50, 1900.
- [Perrone *et al.*, 2019] V. Perrone, H. Shen, MW. Seeger, C. Archambeau, and R. Jenatton. Learning search spaces for Bayesian optimization: Another view of hyperparameter transfer learning. *Advances in Neural Information Processing Systems*, 2019.
- [Sass *et al.*, 2022] R. Sass, E. Bergman, A. Biedenkapp, F. Hutter, and M. Lindauer. DeepCAVE: An interactive analysis tool for automated machine learning. *arXiv:2206.03493*, 2022.
- [Snoek *et al.*, 2012] J. Snoek, H. Larochelle, and R. Adams. Practical bayesian optimization of machine learning algorithms. In *Advances in Neural Information Processing Systems*, 2012.
- [Watanabe, 2023] S. Watanabe. Tree-structured Parzen estimator: Understanding its algorithm components and their roles for better empirical performance. *arXiv:2304.11127*, 2023.
- [Zimmer *et al.*, 2021] L. Zimmer, M. Lindauer, and F. Hutter. Auto-Pytorch: Multi-fidelity metalearning for efficient and robust AutoDL. *Transactions on Pattern Analysis and Machine Intelligence*, 43, 2021.

A Background

In the main paper, we discussed f-ANOVA for one-dimensional effects for simplicity and used concise notations. In this section, we provide the generalized f-ANOVA and discuss more strictly and precisely.

A.1 Notations

In Appendix, we use the following notations for simplicity:

- $[D] := \{1, 2, \dots, D\}$: a set of integers from 1 to D ,
- $s \subseteq [D]$: a subset of $[D]$,
- $\mathcal{P}_s := 2^s$: the power set of s ,
- $\mathcal{P}_{-s} := 2^s \setminus \{s\}$: the power set of s without s itself,
- $\mathcal{S}_s := \{s\}$: a singleton only with $s \subseteq [D]$,
- $\mathcal{S}_d := \mathcal{S}_{\{d\}}$: a singleton only with $\{d\}$,
- $\mathcal{P}_d := \mathcal{P}_{\mathcal{S}_d} = \{\emptyset, \{d\}\}$: the power set of $\{d\}$,
- $\mathcal{X} \subseteq \mathbb{R}^D$: the search space of the function f ,
- $\mathcal{X}_d \subseteq \mathbb{R}$: the domain of the d -th HP,
- $\mathcal{X}_s \subseteq \mathbb{R}^{|s|}$: the subspace of \mathcal{X} built with the dimensions in s ,
- $\mathcal{X}_{-s} \subseteq \mathbb{R}^{D-|s|}$: the complementary space of \mathcal{X}_s on \mathcal{X} ,
- $\mathbf{x}_s \in \mathcal{X}_s$: a vector in \mathcal{X}_s ,
- μ : the Lebesgue measure,
- \mathcal{B}_d : the Borel body over \mathbb{R}^d ,
- $\mathcal{B}_{\mathcal{X}_s} := \mathcal{B}_{|s|} \cap \mathcal{X}_s$: the Borel body over \mathcal{X}_s ,
- $b(\mathbf{x}|A) := \mathbb{I}[\mathbf{x} \in A]$: a binary function that returns 1 if $\mathbf{x} \in A$,
- $u(A) := \frac{1}{\mu(A)}$: the uniform PDF defined on $A \subseteq \mathbb{R}^d$,
- $f(\mathbf{x}|\mathbf{x}_s)$: a function $f(\mathbf{x})$ with the dimensions in $s \subseteq [D]$ are fixed to \mathbf{x}_s ,
- $f_s(\mathbf{x}_s|S)$: the marginal function of f defined on \mathcal{X}_s that considers the interaction effects of dimensions belonging to $S \subseteq \mathcal{P}_s$,

where $d \in [D]$. Notice that the notations in the appendix are slightly different from those in the main paper to be more precise.

A.2 Lebesgue Integral

We first note that the definition of the Lebesgue measure μ changes based on the input for simplicity if not specified although this is abuse of notation. For example, when we take $A \in \mathcal{B}_D \cap \mathcal{X}$ as an input, μ is defined on \mathcal{X} and when we take $A \in \mathcal{B}_{|s|} \cap \mathcal{X}_s$ as an input, μ is defined on \mathcal{X}_s . In this paper, we consistently use the Lebesgue integral $\int_{\mathbf{x} \in \mathcal{X}} g(\mathbf{x}) \mu(d\mathbf{x})$ instead of the Riemann integral $\int_{\mathbf{x} \in \mathcal{X}} g(\mathbf{x}) d\mathbf{x}$; however, $\int_{\mathbf{x} \in \mathcal{X}} g(\mathbf{x}) d\mathbf{x} = \int_{\mathbf{x} \in \mathcal{X}} g(\mathbf{x}) \mu(d\mathbf{x})$ holds if $g(\mathbf{x})$ is Riemann integrable. The only reason why we use the Lebesgue integral is that some functions in our discussion cannot be handled by the Riemann integral, and thus we encourage readers to replace $\mu(d\mathbf{x})$ with $d\mathbf{x}$ if they are not familiar with the Lebesgue integral.

A.3 Generalized f-ANOVA

Suppose we would like to quantify HPI of a function $f(\mathbf{x})$ defined on \mathcal{X} , then global HPI [Hooker, 2007] requires:

1. **Marginal mean:**

$$f_s(\mathbf{x}_s|\mathcal{P}_s) := \int_{\mathbf{x}_{-s} \in \mathcal{X}_{-s}} f(\mathbf{x}|\mathbf{x}_s) \frac{\mu(d\mathbf{x}_{-s})}{\mu(\mathcal{X}_{-s})}, \quad (19)$$

2. **Zero-centered marginal mean:**

$$f_s(\mathbf{x}_s|\mathcal{S}_s) := f_s(\mathbf{x}_s|\mathcal{P}_s) - \sum_{s' \in \mathcal{P}_{-s}} f_{s'}(\mathbf{x}_{s'}|\mathcal{S}_{s'}), \quad (20)$$

3. **Marginal variance:**

$$v_s := \int_{\mathbf{x}_s \in \mathcal{X}_s} f_s(\mathbf{x}_s|\mathcal{S}_s)^2 \frac{\mu(d\mathbf{x}_s)}{\mu(\mathcal{X}_s)}, \quad (21)$$

where $f_s(\mathbf{x}_s|\cdot)$ is a mean function defined on the subspace \mathcal{X}_s . For the case of $s = \emptyset$, as f_\emptyset is the mean of $f(\mathbf{x})$ on \mathcal{X} , $v_0 := v_\emptyset$ becomes *global variance* and it is computed as:

$$v_0 = \int_{\mathbf{x} \in \mathcal{X}} \underbrace{(f(\mathbf{x}) - f_\emptyset)^2}_{:= f_\emptyset(\cdot|\emptyset)} \frac{\mu(d\mathbf{x})}{\mu(\mathcal{X})}. \quad (22)$$

Then global HPI of a set of dimensions s is defined as the fraction v_s/v_0 as it is guaranteed that:

$$v_0 = \sum_{s \in \mathcal{P}_{[D]} \setminus \mathcal{S}_\emptyset} v_s. \quad (23)$$

For more details, see “variance decomposition” in Hooker [2007]. Note that we consistently use f_d as $f_{\mathcal{S}_d}$ and v_d as $v_{\mathcal{S}_d}$.

B Theoretical Details of PED-ANOVA

B.1 Preliminaries

We first provide the following definitions:

Definition 2 (γ -quantile value) Given a quantile $\gamma \in (0, 1]$ and a measurable function $f: \mathcal{X} \rightarrow \mathbb{R}$, γ -quantile value $f^\gamma \in \mathbb{R}$ is a real number such that:

$$f^\gamma := \inf \left\{ f^* \in \mathbb{R} \mid \int_{\mathbf{x} \in \mathcal{X}} \mathbb{I}[f(\mathbf{x}) \leq f^*] \frac{\mu(d\mathbf{x})}{\mu(\mathcal{X})} \geq \gamma \right\}. \quad (24)$$

Definition 3 (γ -set) Given a quantile $\gamma \in (0, 1]$, γ -set \mathcal{X}^γ is defined as $\mathcal{X}^\gamma := \{\mathbf{x} \in \mathcal{X} \mid f(\mathbf{x}) \leq f^\gamma\} \in \mathcal{B}_{\mathcal{X}}$.

Definition 4 (Marginal γ -set PDF) Given the γ -set \mathcal{X}^γ and its γ -set PDF $p(\mathbf{x}|\mathcal{X}^\gamma)$, the marginal γ -set PDF for the d -th dimension is computed as:

$$p_d(\mathbf{x}_d|\mathcal{X}^\gamma) := \int_{\mathbf{x}_{-d} \in \mathcal{X}_{-d}} p(\mathbf{x}|\mathcal{X}^\gamma) \mu(d\mathbf{x}_{-d}). \quad (25)$$

Definition 5 (Pearson divergence [Pearson, 1900]) The Pearson divergence between two PDFs $p(\mathbf{x})$, $q(\mathbf{x})$ is defined as:

$$D_{\text{PE}}(p||q) := \int_{\mathbf{x} \in \mathcal{X}} \left(\frac{p(\mathbf{x})}{q(\mathbf{x})} - 1 \right)^2 q(\mathbf{x}) \mu(d\mathbf{x}). \quad (26)$$

The approximation is usually performed via either Monte-Carlo sampling or the direct estimation [Sugiyama *et al.*, 2013]. Figure 9 intuitively presents how we approximate PED. Throughout this paper, we assume that the support of q includes that of p .

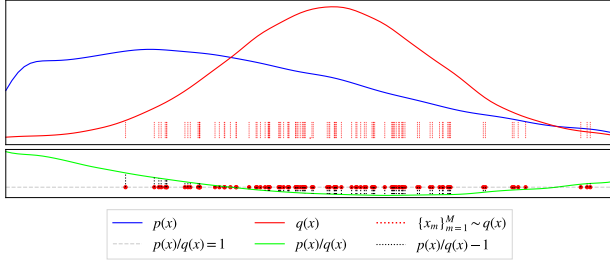


Figure 9: The conceptual visualization of Pearson divergence (PED). **Top:** the two PDFs (red, blue lines) of which we would like to measure PED. **Bottom:** the density ratio of the two PDFs (green line) and the baseline (gray dashed line), which is $p(x)/q(x) = 1$. PED measures the squared average of $p(x)/q(x) - 1$ (the black dotted lines) over the samples from $q(x)$ (red dots) if the density ratio is defined over a continuous space; otherwise we can compute PED by a closed-form.

B.2 Global Hyperparameter Importance

Suppose we would like to analyze a function f , we first introduce the binary function $b(\mathbf{x}|\mathcal{X}^\gamma) = \mathbb{I}[\mathbf{x} \in \mathcal{X}^\gamma]$, which is actually a probability measure. Then the following proposition is derived from this constraint:

Proposition 1 *Given the binary function $b(\mathbf{x}|\mathcal{X}^\gamma)$ and its γ -set PDF $p(\mathbf{x}|\mathcal{X}^\gamma)$, the marginal variance of each dimension $d \in [D]$ is:*

$$v_d = \gamma^2 \int_{x_d \in \mathcal{X}_d} \left(\frac{p_d(x_d|\mathcal{X}^\gamma)}{u(\mathcal{X}_d)} - 1 \right)^2 u(\mathcal{X}_d) \mu(dx_d) \quad (27)$$

$$= \gamma^2 D_{\text{PE}}(p_d(\cdot|\mathcal{X}^\gamma) \| u(\mathcal{X}_d)).$$

The proof is provided in Appendix C.2. It measures PED between the uniform PDF $u(\mathcal{X}_d) = p_d(x_d|\mathcal{X})$ and the marginal γ -set PDF $p_d(x_d|\mathcal{X}^\gamma)$. This HPI measure is generalized to higher orders and we show the formulation in Eq. (47) of Appendix C.2. Note that since a non-uniform sampler yields non-uniform \mathcal{D} , it is recommended to use $p_d(x_d|\mathcal{D}^\gamma)$ with $\gamma = 1$ instead of $u(\mathcal{X}_d)$, i.e. $p_d(x_d|\mathcal{D})$, as discussed in detail in Appendix E.2. The difference between using $u(\mathcal{X}_d)$ and $p_d(x_d|\mathcal{D})$ is that while the former shows general HPI in the global space, the latter shows HPI during the search.

B.3 Local Hyperparameter Importance

On top of global HPI, our method can quantify local HPI using the following theorem (equivalent to Theorem 1):

Theorem 2 *Given the binary function $b(\mathbf{x}|\mathcal{X}^{\gamma'})$ and the γ' - and γ -set PDFs $p(\mathbf{x}|\mathcal{X}^{\gamma'})$, $p(\mathbf{x}|\mathcal{X}^\gamma)$ where $\gamma' < \gamma$, the local marginal variance of each dimension $d \in [D]$ is:*

$$v_d^\gamma = \left(\frac{\gamma'}{\gamma} \right)^2 \int_{x_d \in \mathcal{X}_d} \left(\frac{p_d(x_d|\mathcal{X}^{\gamma'})}{p_d(x_d|\mathcal{X}^\gamma)} - 1 \right)^2 p_d(x_d|\mathcal{X}^\gamma) \mu(dx_d)$$

$$= \left(\frac{\gamma'}{\gamma} \right)^2 D_{\text{PE}}(p_d(\cdot|\mathcal{X}^{\gamma'}) \| p_d(\cdot|\mathcal{X}^\gamma)). \quad (28)$$

This formulation also generalizes to higher orders as shown in Eq. (52) of Appendix C.3.

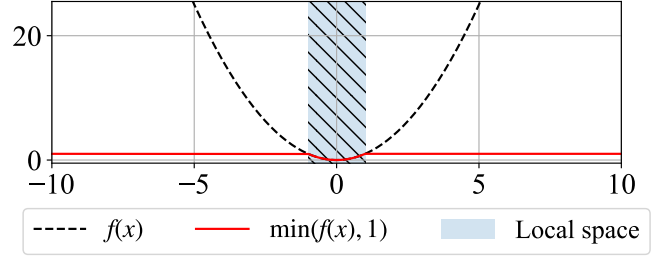


Figure 10: The visualization of the clipped function $g(x) = \min(f(x), 1) = \min(x^2, 1)$. The black dotted line is $f(x)$ and the red solid line is $g(x)$. While global HPI computes the variance over the whole domain $[-10, 10]$, local HPI (**our proposition**) computes the variance only over the blue-shaded domain.

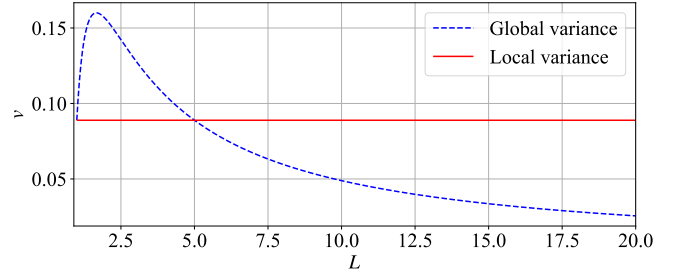


Figure 11: The plots of global/local variances of $g(x)$. The horizontal axis is the domain size L and the vertical axis is the variance of $g(x)$. The blue dashed line shows the global variance and the red solid line shows the local variance. Only the global variance changes depending on the search space design.

B.4 Why Cannot Prior Works Measure Local Importance?

In this section, we analytically describe why the prior works [Hutter *et al.*, 2014; Biedenkapp *et al.*, 2018] cannot local HPI correctly. Note that we take over the notations from the main paper in this section.

B.4.1 Case I: Analysis of Clipped Functions

As mentioned in Section 2.3, Hutter *et al.* [2014] proposed global HPI on a clipped function $g(x) := \min(f(x), f^*)$ as local HPI. However, since global HPI on the clipped function is still affected by the search space design, this is also not a local HPI measure. To illustrate our implication, we would like to present a simple example. Suppose we would like to compute global HPI of $g(x) := \min(x^2, 1)$ defined on $[-L, L]$ as visualized in Figure 10. Then the global mean and the global variance of $g(x)$ are computed as follows:

$$m^{\text{global}}(L) := \frac{1}{2L} \int_{-L}^L g(x) dx = 1 - \frac{2}{3L},$$

$$v^{\text{global}}(L) := \frac{1}{2L} \int_{-L}^L (g(x) - m^{\text{global}}(L))^2 dx \quad (29)$$

$$= \frac{4}{3L} \left(\frac{2}{5} - \frac{1}{3L} \right).$$

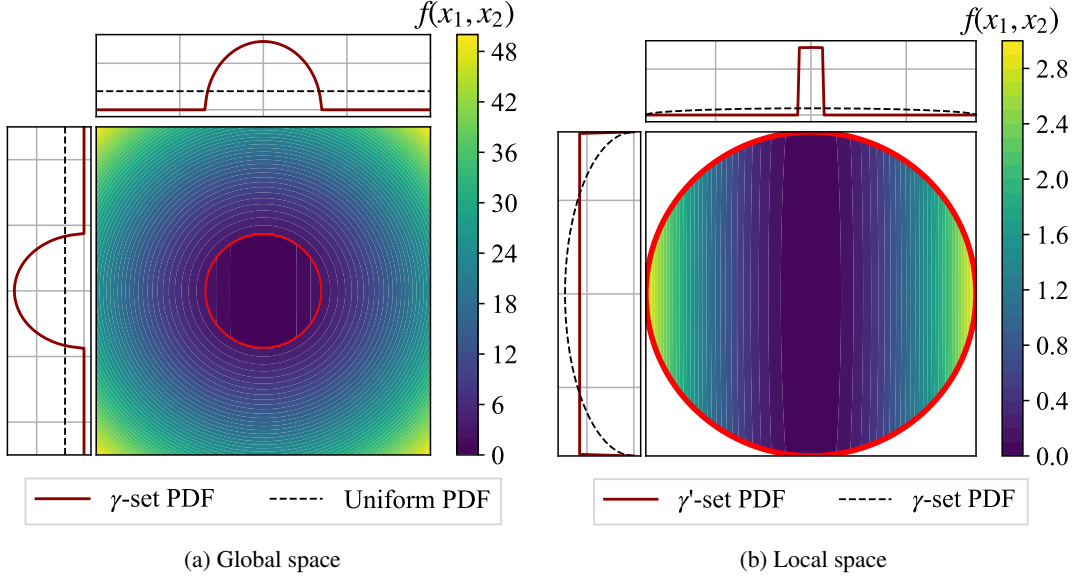


Figure 12: The normalized contour plots of the function (darker is better) in Eq. (31) in both global and local spaces. The function is defined on $[-5, 5] \times [-5, 5]$ and the local space is defined as $f(x_1, x_2) < f^\gamma = 3$, which is $x_1^2 + x_2^2 < 3$. The red circle on the global space represents the local space. The red and black-dashed plots on each side of the figures show the marginal γ -set PDFs and the uniform PDFs in each space. **Left:** the visualization of the global space. Since the marginal γ -set ($\gamma = (\sqrt{3})^2\pi/100 \simeq 0.1$) PDFs for each dimension have the same shape, both dimensions are equally important. **Right:** the visualization of the local space. We took $\gamma' = 0.01$. While the marginal γ' -set for x_1 sharply peaks at the center (**Top** in (b)), that for x_2 does not (**Left** in (b)). It implies that x_1 is more important in the local space.

On the other hand, if we limit the integral to the local space (see the blue-shaded domain in Figure 10), which is $\{x \in [-L, L] \mid f(x) < 1\} = [-1, 1]$, the local mean and the local variance are computed as follows:

$$\begin{aligned} m^{\text{local}} &:= m^{\text{global}}(1) = \frac{1}{3}, \\ v^{\text{local}} &:= v^{\text{global}}(1) = \frac{4}{45}. \end{aligned} \quad (30)$$

Note that our method computes the integral of $\mathbb{I}[x \in [-1, 1]]$ instead of $g(x)$, but we calculated the integral of $g(x)$ here to show the difference from the original proposition. Figure 11 shows the variation in the global variance (the local f-ANOVA by Hutter *et al.* [2014]) in Eq. (29) with respect to the search space design variable L . As can be seen, while the local variance is constant, the global variance dynamically changes. It implies that the prior work cannot strictly quantify HPI locally. The problem is that when we compute the global variance of $g(x)$, the variance v quickly decays as the domain size L becomes larger. It means that HPI in some dimensions might be severely underestimated if we use global HPI on the transformed function such as $g(x)$. For this reason, it is important to limit the integral to a local space.

B.4.2 Case II: Analysis of Dynamically Changing HPI

In this section, we provide a simple example where local HPI matters, but cannot be quantified by the prior work [Biedenkapp *et al.*, 2018] and analytically show the prior work cannot quantify local HPI as intended. We analytically apply Eqs. (2)–(4) (global HPI) and Eqs. (9)–(11)

(our local HPI formula) to the following function:

$$f(x_1, x_2) = \begin{cases} x_1^2 + x_2^2 & (x_1^2 + x_2^2 \geq 3) \\ x_1^2 + \frac{x_2^2}{100} & (\text{otherwise}) \end{cases} \quad (31)$$

where $x_1, x_2 \in [-5, 5]$. The visualization is available in Figure 12 and it is clear that while both x_1, x_2 is equally important in the global space, x_1 is much more important in the local space $\mathcal{X}^\gamma := \{(x_1, x_2) \in [-5, 5] \times [-5, 5] \mid x_1^2 + x_2^2 \leq 3\}$, which is the $\gamma \simeq 0.1$ -set.

We first derive the global marginal variances of each dimension. The global marginal means and the global mean of $f(x_1, x_2)$ are as follows:

$$\begin{aligned} f_1(x_1) &= \begin{cases} x_1^2 + \frac{25}{3} & (|x_1| > \sqrt{3}) \\ x_1^2 + \frac{25}{3} - \frac{33}{500}(3 - x_1^2)^{3/2} & (\text{otherwise}) \end{cases}, \\ f_2(x_2) &= \begin{cases} x_2^2 + \frac{25}{3} & (|x_2| > \sqrt{3}) \\ x_2^2 + \frac{25}{3} - \frac{99}{500}x_2^2\sqrt{3 - x_2^2} & (\text{otherwise}) \end{cases}, \\ m &= \frac{1}{10} \int_{-5}^5 f_1(x_1) dx_1 = \frac{1}{10} \int_{-5}^5 f_2(x_2) dx_2 \\ &= \frac{50}{3} - \frac{891}{40000}\pi. \end{aligned} \quad (32)$$

Then we numerically compute the global marginal variances based on the results.

$$\begin{aligned} v_1 &= \frac{1}{10} \int_{-5}^5 (f_1(x_1) - m)^2 dx_1 \simeq 56.67, \\ v_2 &= \frac{1}{10} \int_{-5}^5 (f_2(x_2) - m)^2 dx_2 \simeq 56.53. \end{aligned} \quad (33)$$

Note that although those values could be analytically computed, we only show the numerical solutions to avoid additional complexities. When using global HPI of PED-ANOVA in Eq. (27), we obtain 2.11 for both dimensions. The results show that both dimensions are almost equally important in the global space as expected. In fact, the marginal γ -set PDFs for each dimension in Figure 12a coincide and this confirms the results.

Now, we derive local HPI of $f(x_1, x_2)$ in \mathcal{X}^γ . We first calculate the scaling factor:

$$\begin{aligned} V_1^\gamma(x_1) &:= \int_{-\sqrt{3-x_1^2}}^{\sqrt{3-x_1^2}} dx_2 = 2\sqrt{3-x_1^2} \\ V_2^\gamma(x_2) &:= \int_{-\sqrt{3-x_2^2}}^{\sqrt{3-x_2^2}} dx_1 = 2\sqrt{3-x_2^2} \\ (\cdot: \mathbb{I}[\mathbf{x} \in \mathcal{X}^\gamma] \Rightarrow x_1^2 + x_2^2 \leq 3). \end{aligned} \quad (34)$$

Then we compute the local marginal means as follows:

$$\begin{aligned} f_1^\gamma(x_1) &= \frac{1}{2\sqrt{3-x_1^2}} \int_{-\sqrt{3-x_1^2}}^{\sqrt{3-x_1^2}} \left(x_1^2 + \frac{x_2^2}{100}\right) dx_2 \\ &= \frac{1}{100} + \frac{299}{300}x_1^2, \end{aligned} \quad (35)$$

$$\begin{aligned} f_2^\gamma(x_2) &= \frac{1}{2\sqrt{3-x_2^2}} \int_{-\sqrt{3-x_2^2}}^{\sqrt{3-x_2^2}} \left(x_1^2 + \frac{x_2^2}{100}\right) dx_1 \\ &= 1 - \frac{97}{300}x_2^2, \end{aligned} \quad (36)$$

Using the local marginal means, the global mean is computed as follows:

$$\begin{aligned} m^\gamma &= \int_{-\sqrt{3}}^{\sqrt{3}} f_1^\gamma(x_1) \underbrace{\frac{2\sqrt{3-x_1^2}}{3\pi}}_{=V_1^\gamma(x_1)/Z} dx_1 \\ &= \int_{-\sqrt{3}}^{\sqrt{3}} f_2^\gamma(x_2) \underbrace{\frac{2\sqrt{3-x_2^2}}{3\pi}}_{=V_2^\gamma(x_2)/Z} dx_2 = \frac{303}{400}. \end{aligned} \quad (37)$$

Note that $2\sqrt{3-x_1^2}/3\pi$, $2\sqrt{3-x_2^2}/3\pi$ are the marginal γ -set PDFs and it refers to $V_d^\gamma(x_d)/Z$ of Eq. (11) in the main paper. Then we yield the marginal variances for each dimension as follows:

$$\begin{aligned} v_1^\gamma &= \int_{-\sqrt{3}}^{\sqrt{3}} (f_1^\gamma(x_1) - m^\gamma)^2 \frac{2\sqrt{3-x_1^2}}{3\pi} dx_1 \\ &= \frac{89401}{160000} \simeq 0.559, \\ v_2^\gamma &= \int_{-\sqrt{3}}^{\sqrt{3}} (f_2^\gamma(x_2) - m^\gamma)^2 \frac{2\sqrt{3-x_2^2}}{3\pi} dx_2 \\ &= \frac{9409}{160000} \simeq 0.0588. \end{aligned} \quad (38)$$

Additionally, local HPI of PED-ANOVA in Eq. (28) yields $v_1^\gamma \simeq 8.97$ and $v_1^\gamma \simeq 0.181$. This shows that x_1 is more

important in the local space and this interpretation can be seen in Figure 12b as well. In fact, while the marginal γ -set PDF for x_2 is close to uniform, that for x_1 sharply peaks at the center. This indicates that x_1 is indeed more important in the local space.

In contrast to our method, the local f-ANOVA based on Eq. (6) obtains the following results:

$$\begin{aligned} m_1 &= \frac{1}{10} \int_{-5}^5 f(x_1, 0) dx_1 = \frac{25}{3}, \\ m_2 &= \frac{1}{10} \int_{-5}^5 f(0, x_2) dx_2 = \frac{25}{3} - \frac{99\sqrt{3}}{500}, \\ v_1 &= \frac{1}{10} \int_{-5}^5 (f(x_1, 0) - m_1)^2 dx_1 = \frac{500}{9} \simeq 55.6, \\ v_2 &= \frac{1}{10} \int_{-5}^5 (f(0, x_2) - m_2)^2 dx_2 \simeq 60.5, \end{aligned} \quad (39)$$

where we plugged in the optimal solution $\mathbf{x}^{\text{opt}} = [0, 0]^\top$ for $f(x_1, x_2)$ to Eq. (6). The conclusion drawn from the results is that both dimensions are almost equally important in the local space; however, it clearly contradicts the intuition drawn from Figure 12b.

B.5 Riemann Split vs Lebesgue Split

As discussed in Section 3.1, the Lebesgue split reduces the number of control parameters and allows us to focus on the analysis in promising domains. Furthermore, it provides more reliable quantification because the subspaces obtained by the Lebesgue split guarantee to have observations while those by the Riemann split do not. This also leads to the debias in the quantification incurred by sampling bias [Moosbauer *et al.*, 2021]. In principle, the sampling bias is caused when observations are not generated from a uniform sampler, e.g. when using Bayesian optimization. It may lead to incorrect quantification of HPI because the integral of f-ANOVA in Eqs. (2)–(4) taken over the uniform PDF. However, as the local HPI in Eqs. (9)–(11) takes the integral over the distribution built by the observations, the sampling bias can be removed. Note that the difference between using $u(\mathcal{X}_d)$ and $p_d(x_d|\mathcal{D})$ is that while the former shows general HPI in the global space, the latter shows HPI during the search and we discuss more details in Appendix E.2. The sampling bias is a big problem in the Riemann split because it does not guarantee to have observations in the specified subspace. It implies that when we do not have no observations near or inside the specified subspace, the surrogate model could be very unreliable and we could even get zero variances for all the parameters, which means that all the parameters are trivial. The drawback of the Lebesgue split is to not be able to provide an easy-to-understand subspace compared to the Riemann split. Especially when practitioners have a specific subspace in their mind, the Riemann split could be a better choice.

B.6 Benefits of Scale Ignorance

We first note that a function $f(x)$ is higher-is-better in this section, but a function $f(x)$ is lower-is-better in the other

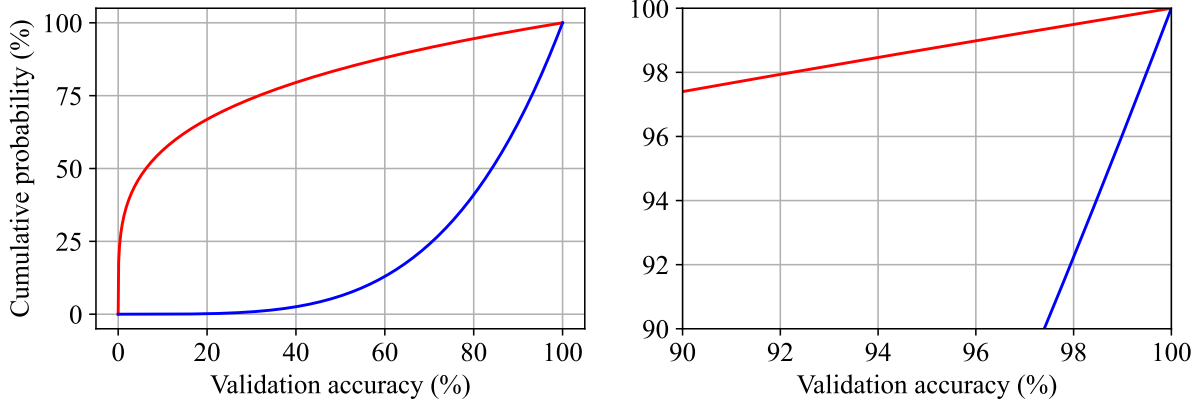


Figure 13: The distributions of two different functions. The horizontal axis shows the function value of $f(\mathbf{x})$ (we consider the validation accuracy of image classification) and the vertical axis shows the cumulative probability of a certain validation accuracy value. For example, the validation accuracy of 60% in the blue line of the left figure is about the bottom 15% and that of 80% the blue line of the left figure is about the bottom 40%. **Left:** the whole range of distributions. The red line shows that the bottom-25% configurations still exhibits the validation accuracy of about 0% and the blue line shows that the bottom-25% configurations already exhibits the validation accuracy of about 70%. **Right:** the magnified figure of the left figure. While the blue line can improve only about 3% from the top-10% to the top (i.e. $\Delta f_1 \simeq 0.03$), the blue line can improve 97% from the bottom to the top-10% (i.e. $\Delta f_2 \simeq 0.97$). For the red line, $\Delta f_1 \simeq 0.65$ and $\Delta f_2 = 0.35$.

sections. As discussed in Section 4.2, the benefit of scale ignorance is to be able to ignore the contribution from the tail. We prepared two functions with different function value distributions in Figure 13. More formally, the distributions show:

$$\mathbb{P}(f^*) := \frac{1}{\mu(\mathcal{X})} \int_{\mathbf{x} \in \mathcal{X}} \mathbb{I}[f(\mathbf{x}) \leq f^*] \mu(d\mathbf{x}). \quad (40)$$

While the red line shows a quick evolution of the validation accuracy at the high cumulative probability domain, the blue line shows a slow evolution. In principle, when a function exhibits a slow evolution at the high cumulative probability domain as in the blue line, the function exhibits a quick evolution at the low cumulative probability domain, and thus the variance is biased toward the variation in the low cumulative probability domain. For example, we are intrinsically interested in what makes difference in the last few percent of the validation accuracy, but not the first trivial 80 ~ 90% variation. More formally, we need to pay attention to:

1. **Variation from bottom:** $\Delta f_1 := \mathbb{P}^{-1}(1 - \gamma) - \mathbb{P}^{-1}(0)$,
2. **Variation from top:** $\Delta f_2 := \mathbb{P}^{-1}(1) - \mathbb{P}^{-1}(1 - \gamma)$.

When $\Delta f_1 \gg \Delta f_2$ as in the blue line, the original f-ANOVA is likely to yield a global variance similar to the scale of Δf_1^2 rather than Δf_2^2 although we cannot mathematically guarantee it. In Section 4.2, we called **variation from bottom** “tail”. As discussed in Appendix D.1, JAHS-Bench-201 has similar distributions as the blue line in Figure 13. PED-ANOVA will not be affected by *variation from bottom* due to the scale ignorance nature and it captures HPI for better performance in the last effort more clearly.

C Proofs

C.1 Assumptions

We assume the following:

1. Objective function $f : \mathcal{X} \rightarrow \mathbb{R}$ is a square-integrable measurable function defined over the compact convex measurable subset $\mathcal{X} \subseteq \mathbb{R}^D$, and
2. The γ -set PDF always exists and $p(\mathbf{x}|\mathcal{X}^\gamma) \propto b(\mathbf{x}|\mathcal{X}^\gamma) := b^\gamma(\mathbf{x}) = \mathbb{I}[\mathbf{x} \in \mathcal{X}^\gamma]$ holds.

Strictly speaking, we cannot guarantee that the γ -set PDF always exists; however, we formally assume that the γ -set PDF exists by considering the empirical distribution and the formal derivative of the step function as the Dirac delta function. As defined above, we use $b^\gamma(\mathbf{x})$ for simplicity in this section.

C.2 Proof of Proposition 1

We first compute the marginal mean of the binary function $b^\gamma(\mathbf{x})$:

$$f_d(x_d|\mathcal{P}_d) := \frac{V_d^\gamma(x_d)}{\mu(\mathcal{X}_{-d})} = \int_{\mathbf{x}_{-d} \in \mathcal{X}_{-d}} b^\gamma(\mathbf{x}|\mathbf{x}_d) \frac{\mu(d\mathbf{x}_{-d})}{\mu(\mathcal{X}_{-d})} \quad (41)$$

where $\mathbf{x}_{-d} \in \mathbb{R}^{D-1}$ is \mathbf{x} without the d -th dimension. We also note that the following holds by definition of the binary function:

$$m = \gamma = \int_{\mathbf{x} \in \mathcal{X}} b^\gamma(\mathbf{x}) \frac{\mu(d\mathbf{x})}{\mu(\mathcal{X})}. \quad (42)$$

Notice that m is the second term of RHS in Eq. (20) because $\mathcal{P}_{-d} = \{\emptyset\}$ holds. Then we first prove the following lemma:

Lemma 1 *The following holds under the assumptions of this section:*

$$\gamma = \int_{x_d \in \mathcal{X}_d} \frac{V_d^\gamma(x_d)}{\mu(\mathcal{X}_{-d})} \frac{\mu(dx_d)}{\mu(\mathcal{X}_d)} = \int_{x_d \in \mathcal{X}_d} \frac{V_d^\gamma(x_d)}{\mu(\mathcal{X})} \mu(dx_d). \quad (43)$$

Proof 1 By definition, the following equality holds:

$$\int_{x_d \in \mathcal{X}_d} \frac{V_d^\gamma(x_d)}{\mu(\mathcal{X}_{-d})} \frac{\mu(dx_d)}{\mu(\mathcal{X}_d)} = \int_{x_d \in \mathcal{X}_d} \int_{\mathbf{x}_{-d} \in \mathcal{X}_{-d}} b^\gamma(\mathbf{x}|x_d) \frac{\mu(d\mathbf{x}_{-d})}{\mu(\mathcal{X}_{-d})} \frac{\mu(dx_d)}{\mu(\mathcal{X}_d)}. \quad (44)$$

Since the Lebesgue measure is a product measure and $b^\gamma(\mathbf{x}) \geq 0$, the Fubini's theorem holds, and thus we obtain the following:

$$\text{LHS} = \int_{\mathbf{x} \in \mathcal{X}} b^\gamma(\mathbf{x}) \frac{\mu(d\mathbf{x})}{\mu(\mathcal{X})} = \gamma \quad (\because \text{Eq. (42)}). \quad (45)$$

This completes the proof.

Using this lemma, we prove Proposition 1.

Proof 2 From the assumption, $b^\gamma(\mathbf{x})$ is proportional to the γ -set PDF $p(\mathbf{x}|\mathcal{X}^\gamma)$, the marginalization of $b^\gamma(\mathbf{x})$ is also proportional to that of the γ -set PDF. From Lemma 1, the scale to equalize this marginalization is $\gamma\mu(\mathcal{X})$; therefore, the marginal γ -set PDF is computed as $p_d(x_d|\mathcal{X}^\gamma) = V_d^\gamma(x_d)/(\gamma\mu(\mathcal{X}))$ and we obtain the following marginal variance:

$$\begin{aligned} v_d &= \int_{x_d \in \mathcal{X}_d} \left(\underbrace{\frac{V_d^\gamma(x_d)}{\mu(\mathcal{X}_{-d})}}_{f_d(x_d|\mathcal{P}_d)} - \underbrace{\gamma}_m \right)^2 \frac{\mu(dx_d)}{\mu(\mathcal{X}_d)} \quad (\because \text{Eq. (4)}) \\ &= \mathbb{E} \left[\left(\frac{V_d^\gamma(x_d)}{\mu(\mathcal{X}_{-d})} - \gamma \right)^2 \right] \\ &= \mathbb{E}[(\gamma\mu(\mathcal{X}_d)p_d(x_d|\mathcal{X}^\gamma) - \gamma)^2] \\ &= \gamma^2 \mathbb{E} \left[\left(\frac{p_d(x_d|\mathcal{X}^\gamma)}{u(\mathcal{X}_d)} - 1 \right)^2 \right] \end{aligned} \quad (46)$$

where we used $u(\mathcal{X}_d) = 1/\mu(\mathcal{X}_d)$ and the expectation is taken with respect to $u(\mathcal{X}_d)$. This completes the proof.

Using Eqs. (19)–(21) and considering the same procedure as in Proposition 1, higher orders of HPI for an arbitrary combination of dimensions $s \subseteq [D]$ can be computed as:

$$\begin{aligned} v_s &= \mathbb{E} \left[\left(\frac{V_s^\gamma(\mathbf{x}_s)}{\mu(\mathcal{X}_{-s})} - \sum_{s' \in \mathcal{P}_{-s}} \frac{V_{s'}^\gamma(\mathbf{x}_{s'})}{\mu(\mathcal{X}_{-s'})} \right)^2 \right] \\ &= \mathbb{E} \left[\left(\frac{\gamma p_s(\mathbf{x}_s|\mathcal{X}^\gamma)}{u(\mathcal{X}_s)} - \sum_{s' \in \mathcal{P}_{-s}} \frac{\gamma p_{s'}(\mathbf{x}_{s'}|\mathcal{X}^\gamma)}{u(\mathcal{X}_{s'})} \right)^2 \right] \\ &\quad \left(\because p_s(\mathbf{x}_s|\mathcal{X}^\gamma) = \frac{u(\mathcal{X})V_s^\gamma(\mathbf{x}_s)}{\gamma} \right) \\ &= \gamma^2 \mathbb{E} \left[\left(\frac{p_s(\mathbf{x}_s|\mathcal{X}^\gamma)}{u(\mathcal{X}_s)} - \sum_{s' \in \mathcal{P}_{-s}} \frac{p_{s'}(\mathbf{x}_{s'}|\mathcal{X}^\gamma)}{u(\mathcal{X}_{s'})} \right)^2 \right] \end{aligned} \quad (47)$$

where the expectation is taken with respect to $u(\mathcal{X}_s)$ and we defined $p_\emptyset = 1$. Note that \mathcal{P}_{-s} includes an empty set \emptyset . For example, when $s = [2]$, the second term becomes:

$$\sum_{s' \in \{S_1, S_2, S_\emptyset\}} \frac{p_{s'}(\mathbf{x}_{s'}|\mathcal{X}^\gamma)}{u(\mathcal{X}_{s'})} = \frac{p_1(x_1|\mathcal{X}^\gamma)}{u(\mathcal{X}_1)} + \frac{p_2(x_2|\mathcal{X}^\gamma)}{u(\mathcal{X}_2)} + 1. \quad (48)$$

Eq. (47) falls back to Eq. (27) when $s = S_d$.

C.3 Proof of Theorem 1

Proof 3 Based on Eq. (10), we first compute the marginal mean of the binary function $b^{\gamma'}(\mathbf{x})$ using $V_d^\gamma(x_d) = \gamma\mu(\mathcal{X})p_d(x_d|\mathcal{X}^\gamma)$:

$$\begin{aligned} f_d^\gamma(x_d|\mathcal{P}_d) &= \int_{\mathbf{x}_{-d} \in \mathcal{X}_{-d}} b^{\gamma'}(\mathbf{x}|x_d) \frac{b^\gamma(\mathbf{x}|x_d)\mu(d\mathbf{x}_{-d})}{V_d^\gamma(x_d)} \\ &= \int_{\mathbf{x}_{-d} \in \mathcal{X}_{-d}} b^{\gamma'}(\mathbf{x}|x_d) \frac{\mu(d\mathbf{x}_{-d})}{V_d^\gamma(x_d)} \\ &\quad (\because \mathcal{X}^{\gamma'} \subseteq \mathcal{X}^\gamma \Rightarrow b^\gamma(\mathbf{x})b^{\gamma'}(\mathbf{x}) = b^{\gamma'}(\mathbf{x})) \quad (49) \\ &= \frac{V_d^{\gamma'}(x_d)}{V_d^\gamma(x_d)} = \frac{\gamma'\mu(\mathcal{X})p_d(x_d|\mathcal{X}^{\gamma'})}{\gamma\mu(\mathcal{X})p_d(x_d|\mathcal{X}^\gamma)} \\ &= \frac{\gamma'}{\gamma} \frac{p_d(x_d|\mathcal{X}^{\gamma'})}{p_d(x_d|\mathcal{X}^\gamma)}. \end{aligned}$$

where we define $f_d^\gamma(x_d|\mathcal{P}_d) = 1$ if $V_d^\gamma(x_d) = 0$. By definition of the binary function, the following holds:

$$m^\gamma = \frac{\gamma'}{\gamma} = \int_{\mathbf{x} \in \mathcal{X}^\gamma} b^{\gamma'}(\mathbf{x}) \frac{\mu(d\mathbf{x})}{\mu(\mathcal{X}^\gamma)}. \quad (50)$$

Using Eqs. (11), (49), (50), the marginal variance is computed as follows:

$$\begin{aligned} v_d^\gamma &= \int_{x_d \in \mathcal{X}_d} \left(\underbrace{\frac{V_d^{\gamma'}(x_d)}{V_d^\gamma(x_d)}}_{f_d^\gamma(x_d|\mathcal{P}_d)} - \underbrace{\frac{\gamma'}{\gamma}}_{m^\gamma} \right)^2 \\ &\quad \times \underbrace{\frac{\int_{\mathbf{x}_{-d} \in \mathcal{X}_{-d}} b^\gamma(\mathbf{x}|x_d)\mu(d\mathbf{x}_{-d})}{\int_{\mathbf{x} \in \mathcal{X}} b^\gamma(\mathbf{x}|x_d)\mu(d\mathbf{x})}}_{p_d(x_d|\mathcal{X}^\gamma) = \frac{V_d^\gamma(x_d)}{\gamma\mu(\mathcal{X})}} \mu(dx_d) \\ &= \left(\frac{\gamma'}{\gamma} \right)^2 \int_{x_d \in \mathcal{X}_d} \left(\frac{p_d(x_d|\mathcal{X}^{\gamma'})}{p_d(x_d|\mathcal{X}^\gamma)} - 1 \right)^2 p_d(x_d|\mathcal{X}^\gamma) \mu(dx_d) \\ &= \left(\frac{\gamma'}{\gamma} \right)^2 \mathbb{E} \left[\left(\frac{p_d(x_d|\mathcal{X}^{\gamma'})}{p_d(x_d|\mathcal{X}^\gamma)} - 1 \right)^2 \right] \end{aligned} \quad (51)$$

where the expectation is taken over $p_d(x_d|\mathcal{X}^\gamma)$. This completes the proof.

Using Eqs. (2)–(4) and considering the same procedure as in Theorem 1, higher orders of HPI for an arbitrary combination of dimensions $s \subseteq [D]$ can be computed as:

$$\begin{aligned} v_s^\gamma &= \mathbb{E} \left[\left(\frac{V_s^{\gamma'}(\mathbf{x}_s)}{V_s^\gamma(\mathbf{x}_s)} - \sum_{s' \in \mathcal{P}_{-s}} \frac{V_{s'}^{\gamma'}(\mathbf{x}_{s'})}{V_{s'}^\gamma(\mathbf{x}_{s'})} \right)^2 \right] \\ &= \mathbb{E} \left[\left(\frac{\gamma' p_s(\mathbf{x}_s|\mathcal{X}^{\gamma'})}{\gamma p_s(\mathbf{x}_s|\mathcal{X}^\gamma)} - \sum_{s' \in \mathcal{P}_{-s}} \frac{\gamma' p_{s'}(\mathbf{x}_{s'}|\mathcal{X}^{\gamma'})}{\gamma p_{s'}(\mathbf{x}_{s'}|\mathcal{X}^\gamma)} \right)^2 \right] \\ &= \left(\frac{\gamma'}{\gamma} \right)^2 \mathbb{E} \left[\left(\frac{p_s(\mathbf{x}_s|\mathcal{X}^{\gamma'})}{p_s(\mathbf{x}_s|\mathcal{X}^\gamma)} - \sum_{s' \in \mathcal{P}_{-s}} \frac{p_{s'}(\mathbf{x}_{s'}|\mathcal{X}^{\gamma'})}{p_{s'}(\mathbf{x}_{s'}|\mathcal{X}^\gamma)} \right)^2 \right] \end{aligned} \quad (52)$$

where the expectation is taken with respect to $p_s(\mathbf{x}_s|\mathcal{X}^\gamma)$. Recall that we defined $p_\emptyset = 1$ and \mathcal{P}_{-s} includes an empty set \emptyset . For example, when $s = [2]$, the second term becomes:

$$\sum_{s' \in \{s_1, s_2, s_\emptyset\}} \frac{p_{s'}(\mathbf{x}_{s'}|\mathcal{X}^{\gamma'})}{p_{s'}(\mathbf{x}_{s'}|\mathcal{X}^\gamma)} = \frac{p_1(x_1|\mathcal{X}^{\gamma'})}{p_1(x_1|\mathcal{X}^\gamma)} + \frac{p_2(x_2|\mathcal{X}^{\gamma'})}{p_2(x_2|\mathcal{X}^\gamma)} + 1. \quad (53)$$

Eq. (52) falls back to Eq. (28) when $s = \mathcal{S}_d$.

C.4 Proof about Discretization Error

In this section, we prove the maximum discretization error of PED and the statement is the following proposition:

Proposition 2 Suppose the function $h(x_d) := (p_d(x_d|\mathcal{X}^{\gamma'})/p_d(x_d|\mathcal{X}^\gamma) - 1)^2$ is integrable and Lipschitz continuous with a Lipschitz constant of $C \in \mathbb{R}_{\geq 0}$ and we discretize the domain of this function in n_d grids at the even interval, then the discretization error of the local marginal variance is bounded by $O(\frac{C}{n_d})$.

Proof 4 We define the domain \mathcal{X}_d as $[L, R]$ ($L, R \in \mathbb{R}, L < R$) and the grid points as $\{g_n\}_{n=0}^{n_d-1} := \{L + ns\}_{n=0}^{n_d-1}$ where $s := (R - L)/(n_d - 1)$ is a step size. Furthermore, we use the notation $p_d^\gamma(x_d) := p_d(x_d|\mathcal{X}^\gamma)$. Since the discretization error is maximized when $h(x_d)$ is monotonically increasing or decreasing with the maximum possible slope of C , the maximum possible discretization error ϵ_{\max} is computed as follows:

$$\begin{aligned} & \frac{\epsilon_{\max}}{\gamma'^2} \\ &:= \sum_{n=0}^{n_d-2} \int_{g_n}^{g_{n+1}} p_d^\gamma(x) ((h(x) + C(x - g_n)) - h(x)) dx \\ &= \sum_{n=0}^{n_d-2} \int_{g_n}^{g_{n+1}} p_d^\gamma(x) C(x - g_n) dx \\ &\leq \sum_{n=0}^{n_d-2} \int_{g_n}^{g_{n+1}} s C p_d^\gamma(x) dx = s C \sum_{n=0}^{n_d-2} \int_{g_n}^{g_{n+1}} p_d^\gamma(x) dx \\ &= s C \int_L^R p_d^\gamma(x) dx = s C \left(\because \int_L^R p_d^\gamma(x) dx = 1 \right) \\ &= \frac{C(R - L)}{n_d - 1}. \end{aligned} \quad (54)$$

From the fact that the maximum discretization error $\epsilon_{\max} = \frac{\gamma'^2 C(R - L)}{n_d - 1}$, it is obvious that the discretization error is bounded by $O(\frac{C}{n_d})$ and this completes the proof.

Note that although our result has a term of the domain size $R - L$, the Lipschitz constant C is inversely proportional to $R - L$ for h , and thus the overall order does not change largely.

D Additional Experiments for Real-World Usecase by JAHS-Bench-201

D.1 Details of JAHS-Bench-201

JAHS-Bench-201 [Bansal et al., 2022] is a collection of surrogate benchmarks for HPO which has one of the largest

search spaces in extant literature. In a surrogate benchmark, we provide HP configurations to a surrogate model, e.g. Random Forest, or XGBoost, and then the surrogate model returns the predicted performance metric values for the corresponding HP configurations. Those surrogates are trained on a set of observations, which are pairs of HP configurations and the performance metric. This is in contrast to tabular benchmarks, which query pre-recorded performance metric values from a static table and, thus, cannot handle continuous parameters, whereas surrogate benchmarks can. In our experiments, we used the grid space in Table 2 with 12 dimensions, resulting in 41M HP configurations. Note that we fixed the fidelity parameters ‘‘Resolution Multiplier’’ and ‘‘Training Epochs’’ in the original paper [Bansal et al., 2022] to 1.0 and 200, respectively. Here, ‘‘Choices used in our experiments’’ shows the lattice points ($N = 41,343,750$) used in our experiments, which includes our discretization of the continuous parameters Learning Rate and Weight Decay from JAHS-Bench-201. This benchmark provides XGBoost surrogate models that predict the validation accuracy (and many other metrics) of neural networks on three different image classification datasets (CIFAR10, Fashion-MNIST, and Colorectal-Histology) with each HP configuration. To train the surrogate models, the authors trained deep neural networks with 161M different HP configurations. In Figure 14, we show the distributions of the validation accuracy on each dataset and those distributions show a slow evolution at the high cumulative probability domain as the blue line in Figure 13.

D.2 Sample Efficiency

In this experiment, we would like to show that it is important to use as many data points as possible to obtain precise interpretation. Figure 15 presents the HPI ratios by each algorithm and their standard error over 10 independent runs. Based on the result of our algorithm, the HPI ratios start to converge from 10^4 training data points. On the other hand, Figure 15 shows that f-ANOVA does not converge with 10^4 data points. It implies that we should use as many data points as possible to analyze benchmark datasets, and thus the scalability of our algorithm is desirable.

D.3 Additional Results of Section 5

In this section, we show the additional results of the analysis on JAHS-Bench-201. Table 3 presents the HPI ratios of each HP on each dataset and Figure 16 visualizes the γ -set PDFs for each HP. As in Section 5, we check the RQs based on the results for each dataset except CIFAR10.

For RQ1, we compare the column (Global 0.1, Ours) to (Global 0.1, Original) and the column (Global 0.01, Ours) to (Global 0.01, Original) in Table 3. Although both PED-ANOVA and f-ANOVA provide similar sets of top HPs in Colorectal-Histology, we yielded different patterns in Fashion-MNIST. Since the γ -set PDFs for Width multiplier are peaked at 16 in Figure 16, Width multiplier should be large in f-ANOVA; however, f-ANOVA did not provide such interpretation. This was probably due to the fact that the performance on

Table 2: The search space of JAHS-Bench-201 and the grid space used in our experiments. `TrivialAugment` [Müller and Hutter, 2021] is a data augmentation method and Edge 1 – 6 follows the NAS-Bench-201 [Dong and Yang, 2020] search space. This grid search space has $7 \times 7 \times 3 \times 3 \times 3 \times 2 \times 5^6 \simeq 41\text{M}$ configurations in total. **Hyperparameter**: the names of each HP. **Parameter type**: the type of each HP. Type is either `continuous`, `discrete`, or `categorical`. **Choices used in our experiments**: the values of each grid used in our experiments. While categorical and discrete parameters take exactly the same grids as in the original benchmark dataset, continuous take 7 grids for each HP to make the dataset size finite.

Hyperparameter	Parameter type	Choices used in our experiments
Learning rate	Continuous	$\{1\text{e-}3, 3\text{e-}3, 1\text{e-}2, 3\text{e-}2, 1\text{e-}1, 3\text{e-}1, 1\text{e-}0\}$
Weight decay	Continuous	$\{1\text{e-}5, 3\text{e-}5, 1\text{e-}4, 3\text{e-}4, 1\text{e-}3, 3\text{e-}3, 1\text{e-}2\}$
Activation function	Categorical	$\{\text{relu}, \text{hardswish}, \text{mish}\}$
TrivialAugment	Categorical	$\{\text{True}, \text{False}\}$
Depth multiplier	Discrete	$\{1, 3, 5\}$
Width multiplier	Discrete	$\{4, 8, 16\}$
Operation 1 – 6	Categorical	$\{\text{skip-connection}, \text{none}, \text{bn-conv}3\times3, \text{bn-conv}1\times1, \text{avgpool}3\times3\}$

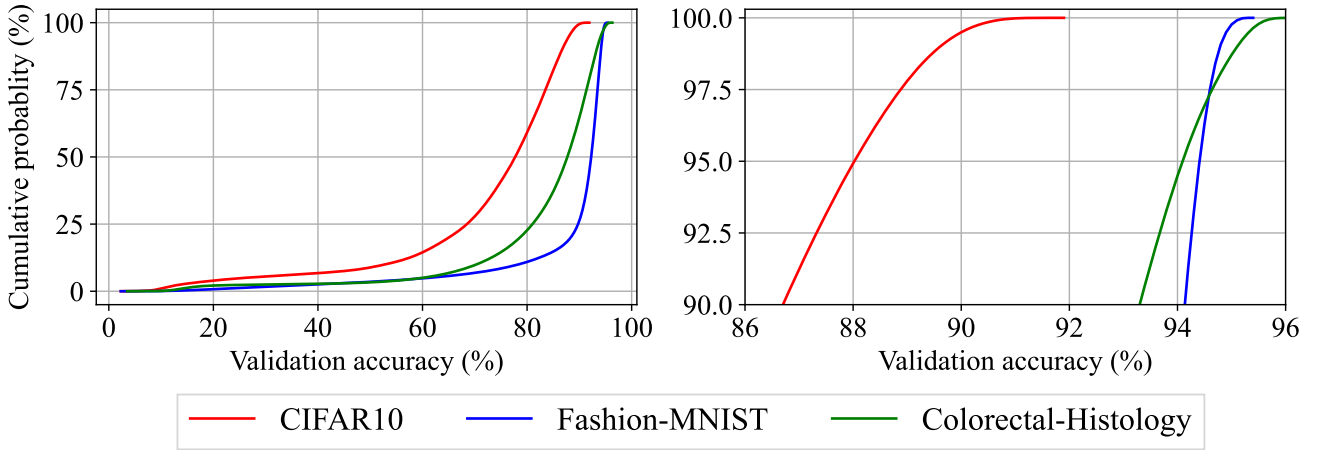


Figure 14: The cumulative distributions of the validation accuracy in each dataset of JAHS-Bench-201. As discussed in Appendix B.6, the distributions exhibit $\Delta f_1 \ll \Delta f_2$. **Left**: the whole range of the distributions. The validation accuracy slowly increases in the high cumulative probability domain, and thus the variation in the high cumulative probability domain is relatively less important as in the blue line of Figure 13. **Right**: the magnified figure of the left figure. This figure tells us that each dataset still has a room for improvement from the top 10%.

Fashion-MNIST is already saturated at the top-10% as seen in Figure 14, and thus our method can provide similar sets of important HPs unless the performance is already saturated at a given quantile γ' .

For RQ2, we compare the column (Global 0.1, Ours) and (Global 0.01, Ours) to (Normal, Original). As discussed in Section 5, we found the misclassification of Op.3 as the most important and of TrivialAugment as the least important HP on CIFAR10 and the same phenomenon happens to both datasets. Therefore, scale invariance indeed helps to successfully identify HPI for HPs that would have been misclassified by the (Normal, Original) setting.

For RQ3, we compare the column (Global 0.01, Ours) to (Local, Ours). We observe that the HPI of Width multiplier drops from the Global 0.01 setting to the Local setting. Simultaneously, the HPI of TrivialAugment increases sharply across the same. This

suggests that optimizing Width multiplier is no longer important when moving from the top-10% to the top-1% performance but optimizing TrivialAugment is very important. The reason behind this change becomes clear when we observe the change in γ -set PDFs of the two HPs in Figure 16. Both the γ -set PDFs for Width multiplier are sharply peaked at 16, indicating that no further optimization is needed on Width multiplier. However, the γ -set PDFs for TrivialAugment only start peaking at the value True for the $\gamma = 0.01$ -set PDF especially in Fashion-MNIST. This clearly demonstrates that local HPI is necessary for deriving the correct interpretation in the top- γ' quantiles, since (Local, Ours) successfully identifies the relative importance of optimizing the two HPs. Last but not least, if both global and local HPI with wished quantiles γ, γ' exhibits low values, removing such HPs, e.g. Activation function, is expected to have a less negative impact although it is insecure to remove HPs, e.g.

Table 3: HPI of Fashion-MNIST and Colorectal-Histology. The ratio of HPI by percentage (**HPI ratio**) computed by $v_d / \sum_{d'=1}^D v_{d'}$. The top-3 HPs are bolded. **Odd cols.** (Original): HPI by original f-ANOVA on $g(x) := \min(f(x), f^{\gamma'})$. **Even cols.** (Ours): HPI by PED-ANOVA.

HPI ratio (%)												
Dataset	Fashion-MNIST						Colorectal-Histology					
Hyperparameter	Normal Original	Global 0.1		Global 0.01		Local	Normal	Global 0.1		Global 0.01		Local
		Ours	Original	Ours	Original	Ours	Original	Ours	Original	Ours	Original	Ours
Learning rate	5.66	12.39	10.04	11.81	15.12	13.30	1.64	16.31	33.66	15.38	31.92	14.14
Weight decay	6.81	6.60	10.37	4.76	15.55	3.15	0.68	2.96	5.07	2.42	3.72	1.58
Activation function	0.76	0.34	0.14	1.19	0.15	2.66	0.01	0.08	0.08	0.20	0.09	0.44
TrivialAugment	0.05	1.59	0.03	9.87	0.06	26.73	0.11	19.70	8.63	20.09	11.50	23.24
Depth multiplier	0.05	1.33	0.07	0.47	0.16	0.01	0.09	2.05	1.88	4.09	1.65	7.47
Width multiplier	0.81	40.65	3.84	38.67	7.10	29.98	0.73	45.33	36.04	39.72	40.46	29.58
Operation 1	15.85	11.54	13.60	14.52	10.59	11.50	11.33	3.25	2.24	3.96	1.66	4.54
Operation 2	1.62	3.93	1.56	6.54	1.73	7.43	4.85	1.36	0.90	1.96	0.75	2.44
Operation 3	42.41	10.34	35.74	4.61	26.48	0.72	64.26	5.16	8.85	6.60	6.03	7.92
Operation 4	0.36	1.68	0.21	2.26	0.31	3.07	0.12	0.47	0.25	0.39	0.30	0.30
Operation 5	3.11	0.91	1.97	0.42	1.29	0.12	4.72	0.72	0.57	1.41	0.55	2.78
Operation 6	22.51	8.69	22.41	4.88	21.46	1.32	11.47	2.61	1.82	3.78	1.36	5.57

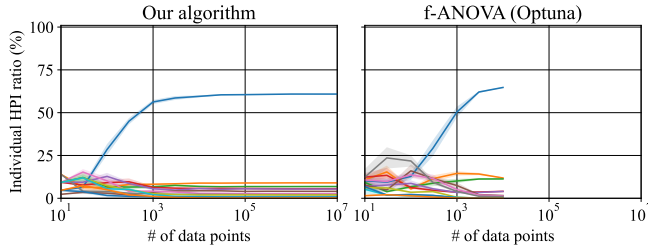


Figure 15: The plot for the sample efficiency of our algorithm using CIFAR10 in JAHS-Bench-201. The horizontal axis is the number of data points to be used in the training of our algorithm (PED-ANOVA) and f-ANOVA, and the vertical axis is the HPI ratio of each HP. The colors of plots were determined by the ranking of HPI in each setting and the weak color band shows the standard error of each HPI ratio over 10 independent runs. **Left:** the results for our algorithm. The HPI ratio starts to converge from 10^4 data points. **Right:** the results for f-ANOVA by Optuna. Due to the expensive computation, we could run only until 10^4 data points and it did not exhibit convergence.

TrivialAugment in Fashion-MNIST, only by looking at global HPI.

E Practical Usecases and Limitations

In this section, we first discuss the advantages and the limitations of our method and then describe the usecases of our method.

E.1 Advantages and Limitations

We list the advantages and limitations, which are not discussed in the main paper. The advantages of our method are that:

1. our method can handle multi-output functions and classification problems because we can measure HPI as long as the objective function can be divided by a specific threshold,

2. the meaning of HPI, which is how important each HP is to achieve the top- γ' quantile, is more clear compared to global f-ANOVA [Hutter *et al.*, 2014],
3. we can handle infinity and missing values without pre-processing thanks to the scale ignorance nature, and
4. the implementation is very simple.

On the other hand, the limitations of our method are that:

1. since the computation of higher orders of HPI requires exponential amounts of time complexity $O(\prod_{d \in s} n_d^2)^3$ if we analyze the interaction in \mathcal{X}_s , our method is not suitable for the approximation of higher order HPI with many grids n_d ,
2. the exact percentage, i.e. v_s/v_0 , is not available in high dimensions because it is hard to obtain the precise variance v_0 , i.e. the highest order HPI, and
3. the marginal objective function (see Figure 1 in Hutter *et al.* [2014]) is not available (instead, we yield distributional visualizations as in Figure 7).

Note that even when we do not have v_0 , the ratio between two marginal variances $v_d/v_{d'}$ have the same meaning as the ratio of percentages. $(v_d/v_0)/(v_{d'}/v_0) = v_d/v_{d'}$.

E.2 Post-Hoc Analysis of HPO

While post-hoc analysis of HPO is an obvious application for our method, we would like to note that the appropriate usage of our method is to apply local HPI with $\gamma = 1$ rather than to apply global HPI in Eq. (27). More specifically, we should use $p_d(x_d|\mathcal{D})$, which is a KDE built by the whole observations \mathcal{D} , instead of $u(\mathcal{X}_d)$. This relates to the sampling bias of (non-random) HPO methods [Moosbauer *et al.*, 2021]. For example, since Bayesian optimization tries to exploit knowledge, the samples would not be generated from the uniform distribution and they concentrate in local spaces. Therefore, $p_d(x_d|\mathcal{D})$ is often dissimilar to the uniform PDF

³We can reduce the complexity with some efforts or Monte-Carlo sampling.

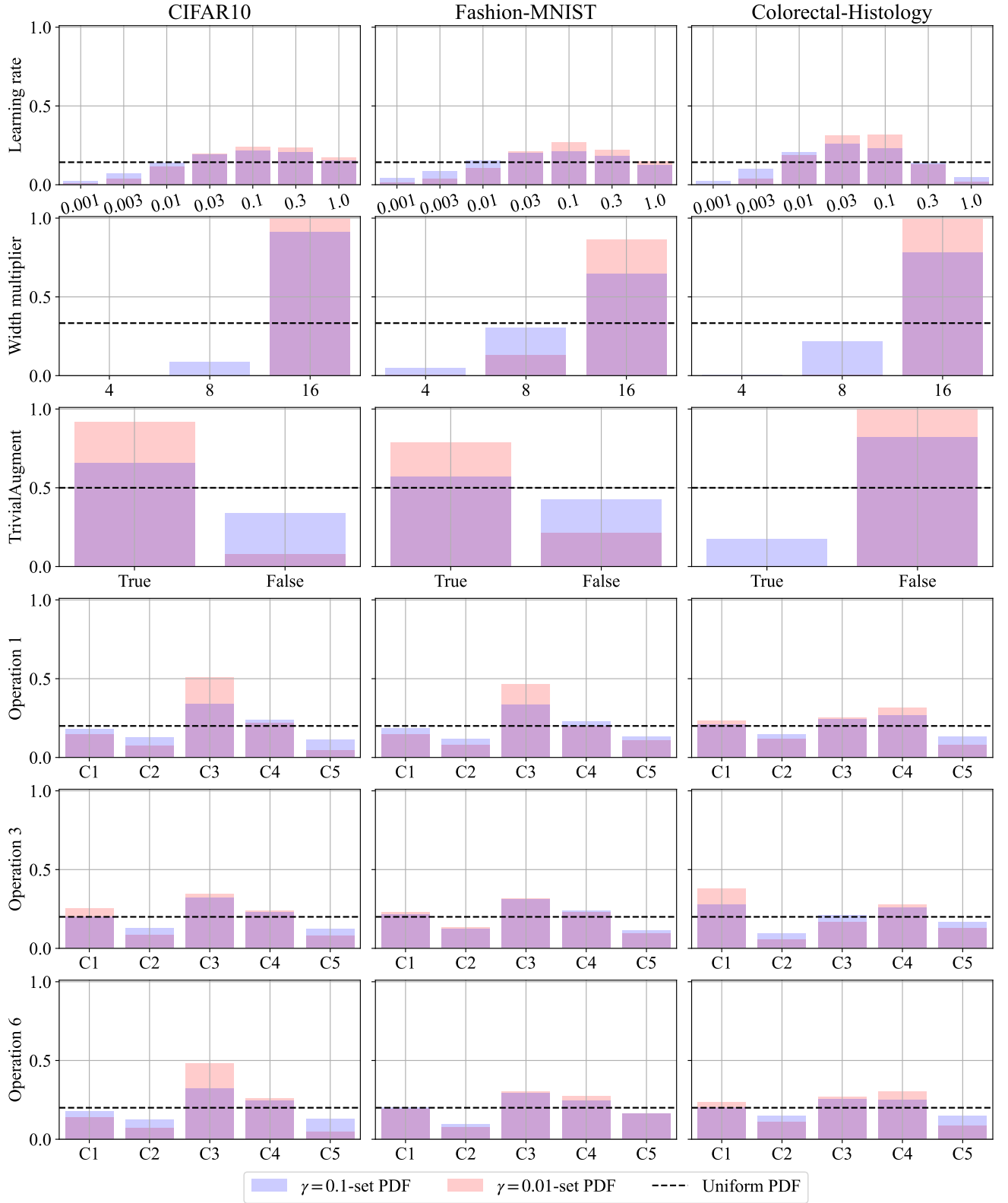


Figure 16: The distributions of important HPs in JAHs-Bench-201. The left, center, and right columns correspond to the results on CIFAR10, Fashion-MNIST, and Colorectal-Histology. The red shadows show the $\gamma = 0.01$ -set PDFs, the blue shadows show the $\gamma = 0.1$ -set PDFs, and the black dashed lines show the uniform PDFs. PED between a black line and a blue shadow is $\text{Global } 0.1$, PED between a black line and a red shadow is $\text{Global } 0.01$, and PED between a red shadow and a blue shadow is Local in Table 3. Notice that C1 – C5 correspond to the order of Table 2 and the overlap between the red and the blue shadows looks purple although they are separated shadows.

$u(\mathcal{X}_d)$ and global HPI in Eq. (27) is biased. When applying PED-ANOVA to samples obtained by Bayesian optimization, high HPI in global HPI indicates that the corresponding HP was easy to optimize even with random search, and high HPI in local HPI with $\gamma = 1$ indicates that the corresponding HP was particularly paid attention to by the sampler. If the goal of the analysis is to identify easy-to-find important HPs, global HPI is appropriate, but if the goal of the analysis is to identify HPs that should be intensively searched, local HPI with $\gamma = 1$ is more appropriate.

In the same vein, we can apply our method to the results of constrained optimization. Typically, we would like to know the HPI in feasible domains. In such a case, we first build the PDF for feasible domains $p_d(x_d|\mathcal{X}_{d,\text{feasible}})$ as local space and we define another PDF $p_d(x_d|\mathcal{X}_{d,\text{feasible}}^\gamma)$, e.g. the PDF of the top- γ -quantile configurations in feasible domains. Then we can compute HPI via PED.

E.3 Search Space Reduction

Our method is useful for search space designs and we would like to discuss the possibility using Figure 7 in Section 4. In the figures, we presented the uniform PDF, γ -set PDFs, and γ' -set PDFs built using the random samples where $\gamma = 0.1$, $\gamma' = 0.01$. We could approach search space reduction from two perspectives: (1) domain reduction of each HP using global HPI and (2) HP selection using local HPI.

For the domain reduction, we need to pay attention to HPs with higher global HPI. In this example, x_1 and x_2 have higher global HPI, and both γ -set PDFs have a peak. Practitioners could sample these HPs only from the domains where the γ -set PDFs exhibit a larger value than the uniform PDF, i.e. $p_d(x_d|\mathcal{D}^\gamma) \geq u_d$.

On the other hand for the HP selection, we need to pay attention to HPs with low HPI both in the local and global spaces. For example, while we can conclude that x_3, x_4 are not important if we rely only on global HPI, x_3 is more important than x_1 in the local space as seen in the figure. For this reason, we should not discard x_3 ; however, as the local HPI of x_4 is small and close to zero, it makes sense to remove x_4 from the search space and fixes x_4 to a default value. Note that it is also not appropriate to discard HPs with low HPI only in the local space because low local HPI just implies that the HPs have a similar trend both in the global and local spaces and the HPs are likely to have more interaction effects compared to the other HPs.

E.4 Exploratory Data Analysis

When we have a dataset $\{(x_n, y_n)\}_{n=1}^N$, we can first define a KPI $y^* := y^\gamma$ and pick the data points such that $y_n \leq y^*$ and define it as \mathcal{D}^γ . Then we obtain the marginal γ -set PDFs $p_d(x_d|\mathcal{D}^\gamma)$ for each feature in the global scale. By plotting those PDFs independently, we can know what features might lead to a good KPI in which ranges and we can also know what features might not affect the KPI.

For the usage of local HPI, first recall that $\mathcal{X}^\gamma, \mathcal{X}^{\gamma'}$ only require $\mathcal{X}^{\gamma'} \subseteq \mathcal{X}^\gamma$, and thus we can define local spaces such that $\mathcal{D}^\gamma = \{x_n | x_n \in \mathcal{D}, y^{\gamma_1} \leq y_n \leq y^{\gamma_2}\}$ and $\mathcal{D}^{\gamma'} = \{x_n | x_n \in \mathcal{D}, y^{\gamma'_1} \leq y \leq y^{\gamma'_2}\}$ where $y^{\gamma_1} \leq y^{\gamma'_1} \leq$

$y^{\gamma'_2} \leq y^{\gamma_2}$. This analysis allows practitioners to know what HPs might be the key to improving the KPI in the local space.

References

- [Bansal *et al.*, 2022] A. Bansal, D. Stoll, M. Janowski, A. Zela, and F. Hutter. JAHS-Bench-201: A foundation for research on joint architecture and hyperparameter search. In *Advances in Neural Information Processing Systems Datasets and Benchmarks Track*, 2022.
- [Biedenkapp *et al.*, 2018] A. Biedenkapp, J. Marben, M. Lindauer, and F. Hutter. CAVE: Configuration assessment, visualization and evaluation. In *International Conference on Learning and Intelligent Optimization*, 2018.
- [Dong and Yang, 2020] X. Dong and Y. Yang. NAS-Bench-201: Extending the scope of reproducible neural architecture search. *arXiv:2001.00326*, 2020.
- [Hooker, 2007] G. Hooker. Generalized functional ANOVA diagnostics for high-dimensional functions of dependent variables. *Journal of Computational and Graphical Statistics*, 16, 2007.
- [Hutter *et al.*, 2014] F. Hutter, H. Hoos, and K. Leyton-Brown. An efficient approach for assessing hyperparameter importance. In *International Conference on Machine Learning*, 2014.
- [Moosbauer *et al.*, 2021] J. Moosbauer, J. Herbringer, G. Casalicchio, M. Lindauer, and B. Bischl. Explaining hyperparameter optimization via partial dependence plots. *Advances in Neural Information Processing Systems*, 2021.
- [Müller and Hutter, 2021] SG. Müller and F. Hutter. TrivialAugment: Tuning-free yet state-of-the-art data augmentation. In *International Conference on Computer Vision*, 2021.
- [Pearson, 1900] K. Pearson. On the criterion that a given system of deviations from the probable in the case of a correlated system of variables is such that it can be reasonably supposed to have arisen from random sampling. *Philosophical Magazine and Journal of Science*, 50, 1900.
- [Sugiyama *et al.*, 2013] M. Sugiyama, S. Liu, MC. Du Plessis, M. Yamanaka, M. Yamada, T. Suzuki, and T. Kanamori. Direct divergence approximation between probability distributions and its applications in machine learning. *Journal of Computing Science and Engineering*, 7, 2013.